

ISTANBUL TECHNICAL UNIVERSITY ★ ENERGY INSTITUTE

**CUBIC NODAL EXPANSION METHOD FOR THE RADIAL
SOLUTION OF THE NEUTRON DIFFUSION EQUATION
IN CYLINDRICAL GEOMETRY**

**M. Sc. Thesis by
Ahmet İlker TOPUZ**

Department: Energy Science and Technology

Programme: Energy Science and Technology

JANUARY 2010

**CUBIC NODAL EXPANSION METHOD FOR THE RADIAL
SOLUTION OF THE NEUTRON DIFFUSION EQUATION
IN CYLINDRICAL GEOMETRY**

**M. Sc. Thesis by
Ahmet İlker TOPUZ
(301071002)**

**Date of submission: 11 December 2009
Date of defence examination: 28 January 2010**

**Supervisor (Chairman) : Prof. Dr. Atilla ÖZGENER (ITU)
Members of the Examining Committee : Prof. Dr. Melih GEÇKİNLİ (ITU)
Prof. Dr. Cemal YILDIZ (ITU)**

JANUARY 2010

**3. DERECE NODAL AÇILIM METODUNUN SİLİNDİR
GEOMETRİDE NÖTRON DİFÜZYON DENKLEMİNİN
RADYAL BİLEŞKESİNE UYGULANMASI**

**YÜKSEK LİSANS TEZİ
Ahmet İlker TOPUZ
(301071002)**

**Tezin Enstitüye Verildiği Tarih: 11 Aralık 2009
Tezin Savunulduğu Tarih: 28 Ocak 2010**

**Tez Danışmanı : Prof. Dr. Atilla ÖZGENER (İTÜ)
Diğer Jüri Üyeleri : Prof. Dr. Melih GEÇKİNLİ (İTÜ)
Prof. Dr. Cemal YILDIZ (İTÜ)**

OCAK 2010

FOREWORD

I represent my thanks to Prof. Dr. Atilla Özgener for his guidance in the way of this thesis development. Additionally, special thanks welcome to Mehmet Mercimek for the contributions to different parts of the study. I would like to dedicate this work to my first advisor Prof. Dr. Akif Atalay, my dear grandfather İbrahim Öztoprak, my dear grandmother Zübeyde Topuz, and my dear grandfather Ahmet Topuz who passed away during my graduate education. Rest in peace...

December 2009

Ahmet İlker TOPUZ

Physicist

TABLE OF CONTENTS

FOREWORD	v
TABLE OF CONTENTS	vii
LIST OF ABBREVIATIONS	ix
LIST OF TABLES	x
LIST OF FIGURES	xi
LIST OF SYMBOLS	xii
SUMMARY	xiii
ÖZET	xv
1. INTRODUCTION	1
1.1 Diffusion Approximation	1
1.2 Nodal Expansion Method	5
1.3 Objectives of the Work	6
2. NODAL FORMALISM IN CYLINDRICAL GEOMETRY	9
2.1 Node Averaged Quantities and Moments	9
2.2 Cubic Nodal Expansion Method	11
2.2.1 Construction of Polynomial Basis	11
2.2.2 Determination of Expansion Coefficients	14
2.3 Fick's Law	16
2.4 Nodal Balance Equation	20
2.5 Weighted Residual Process - First Moment of Diffusion Equation	21
2.6 Formation of Iteration Matrix	25
2.6.1 Discretized Terms Revisited	25
2.6.2 Final Aspect of the Equations	26
2.6.3 Response Matrix For Reflected-Vacuum Boundary Condition	26
3. NUMERICAL APPLICATIONS	29
3.1 One-Group, Bare, Homogeneous Reactor	29
3.1.1 Analytical Solution	29
3.1.2 Geometrical Discretization(2 nodes)	32
3.1.3 CNEMR and QFEMR Results	33
3.2 One-Group, Reflected Reactor	37
3.2.1 Analytical Solution	37
3.2.2 CNEMR and QFEMR Results	41
3.3 Two-Group, Bare, Homogeneous Reactor	45
3.3.1 Analytical Solution	45
3.3.2 CNEMR and QFEMR Results	48
3.4 TRIGA MARK II Reactor	51
4. CONCLUSION	57

REFERENCES	59
APPENDIX A A MANUAL FOR CNEMR	61
A.1 Input List	61
A.2 Description of CNEMR Subroutines	62
APPENDIX B COMPUTER PROGRAMS	65
RESUME	67

LIST OF ABBREVIATIONS

FDM	: Finite Difference Method
FEM	: Finite Element Method
NEM	: Nodal Expansion Method
ODE	: Ordinary Differential Equation
RHS	: Right Hand Side

LIST OF TABLES

	<u>Page</u>
Table 3.1 : Iteration Steps of Newton's Method for the Solution of (3.7)	31
Table 3.2 : Radii and Related Surface Areas.....	32
Table 3.3 : k_{eff} Results of QFEMR and CNEMR Programs	33
Table 3.4 : Average Fluxes and Respective Errors	36
Table 3.5 : Iteration Results of Newton Method.....	39
Table 3.6 : Effective Multiplication Factors Calculated by 3 Methods	41
Table 3.7 : Average Fluxes with Their Errors in the Fuel and the Reflector	44
Table 3.8 : Iteration Steps in Two-Group Problem.....	47
Table 3.9 : Results of QFEMR and CNEMR Programs for Two-Group Reactor ..	48
Table 3.10 : Homogenized Fast Group Cross-Sections for TRIGA Reactor	52
Table 3.11 : Homogenized Thermal Group Cross-Sections for TRIGA Reactor	52
Table 3.12 : CNEMR k_{eff} Results for Different Meshes in TRIGA Reactor.....	53
Table 3.13 : Ring Averaged Fluxes of TRIGA Reactor.....	55

LIST OF FIGURES

	<u>Page</u>
Figure 1.1 : Geometry for derivation	2
Figure 1.1 : Extrapolation Distance	5
Figure 2.1 : Nodal Mesh Imposed on One-dimensional Cylindrical Domain	10
Figure 2.2 : Multigrid of Radial Component in Cylindrical Domain	10
Figure 2.2 : Variation of the Polynomials.....	13
Figure 3.1 : One-dimensional, Bare, Homogeneous, Cylindrical Reactor	29
Figure 3.2 : Cylindrical Reactor with Two Nodes	32
Figure 3.3 : k_{eff} Results of FEM and NEM	34
Figure 3.4 : k_{eff} %error Variation	35
Figure 3.5 : Flux Distributions Along the Radial Distance.....	36
Figure 3.6 : Variation of k_{eff} with Respect to Total Number of Nodes	42
Figure 3.7 : k_{eff} %error Variation	43
Figure 3.8 : Flux Distribution in the Reflected Reactor.....	44
Figure 3.9 : k_{eff} Results of FEM and NEM	49
Figure 3.10 : k_{eff} %error Variation	50
Figure 3.11 : Fast and Thermal Flux Distributions.....	50
Figure 3.12 : ITU TRIGA MARK II Reactor Core Diagram	51
Figure 3.13 : TRIGA Reactor Flux Distribution (CNEMR).....	54
Figure 3.14 : TRIGA Reactor Flux Distribution (Linear QFEMR).....	55

LIST OF SYMBOLS

$\vec{J}_g(\vec{r})$: Neutron current density vector for group g
D^g	: Diffusion coefficient for group g
ϕ_g	: Neutron flux for group g
$\phi_{i,n}$: n^{th} Moment of Neutron flux
w_n	: n^{th} Weight Function
Σ_r	: Macroscopic removal cross-section
Σ_a	: Macroscopic absorption cross-section
$\Sigma_{s,g \rightarrow g'}$: Macroscopic scattering cross-section from group g to group g'
Σ_f	: Macroscopic fission cross-section
k_{eff}	: Effective multiplication factor
χ	: Fission spectrum
ν	: Average number of neutrons released per fission
Q	: Neutron source
$r_{i-1/2}, r_{i+1/2}, r_i$: Radii at node edges and center respectively
Δ_i	: i^{th} node width
j^+	: Right-going partial current
j^-	: Left-going partial current
$S_{i+1/2}, S_{i-1/2}, S_i$: Surface areas at node edges and center respectively
ξ	: Normalized variable
a_l	: Expansion coefficients for polynomial of l^{th} order
ϵ	: Convergence parameter
B	: Buckling term
J_0, J_1	: Bessel functions of first kind, zeroth and first order respectively
w_f	: Recoverable energy per fission
$\bar{\phi}$: Average flux
λ	: Maximum eigenvalue, k_{eff}
I_0, K_0, I_1, K_1	: Zeroth and first order modified Bessel functions of first and second kind respectively

CUBIC NODAL EXPANSION METHOD FOR THE RADIAL SOLUTION OF THE NEUTRON DIFFUSION EQUATION IN CYLINDRICAL GEOMETRY

SUMMARY

The core calculations of nuclear reactors are based on two fundamental theories: diffusion and transport. The transport equation determines position, time, angle and energy dependent descriptions; however, it is also complicated. On the other hand, diffusion is an approximation to the transport theory, and solution is easier when compared to the transport equation. That's why it is more practical for coarse reactor calculations. When the energy spectrum of neutrons is taken into consideration, one can divide the energy of the neutrons in the reactor core into multigroups. By the way, the multigroup neutron diffusion equation is expected to be solved in Reactor Physics.

Nowadays, many methods have been developed for the solution of multigroup neutron diffusion. These methods are classified as analytical, numerical and semi-analytical.

When development of the nuclear engineering is observed, the most common numerical methods, which had been used till 70s, were FDM and FEM. The intersection point of these two methods was the inconvenience to the computer configurations of the period due to high computer memory requirement. Especially, FDM was remarked as an expensive method, for it needs fine and condensed mesh.

Since 70s, Nodal Methods, which have owned their place in nuclear engineering, take attention with their successes in three classes of mathematical methods. The numerical method called as NEM was very useful thanks to its coarse mesh property in contrast to its alternatives FDM and FEM. Moreover, NEM becomes the most popular method of the last 35 years due to its nodes some 20 times greater than FDM cells when FDM system is formed by thousands or millions components, and the lower usage of the computer memory with respect to FEM.

NEM is a numerical polynomial expansion method possessing similar mathematical basis with FEM. Depending on the degree of the polynomials, it may be classified as low ($n=2$) or high ($n\geq 3$) order expansion. For low order expansions, Fick's law and neutron balance equation are sufficient in order to solve the system. In contrast, high order expansions require the determination of the neutron flux moments. An n^{th} order expansion needs to have $n+1$ basis polynomials and expansion coefficients. For high order expansions, $n-2$ neutron moments should be calculated, and also weighted residuals process is applied $n-2$ times.

In the present study, Cubic NEM is applied for the radial solution of neutron diffusion equation in cylindrical geometry. After the formation of the algebraic system, the CNEMR code is built in order to obtain the solutions. CNEMR is a FORTRAN code which is able to calculate the effective neutron multiplication constant, intra-nodal averaged fluxes, and the general averaged flux of the core. The

data obtained from CNEMR is compared with Quadratic NEM, linear FEM, and Quadratic FEM.

The comparisons reveals that convergence of Cubic NEM to acceptable values is faster than the compared methods in one-group problems, and the augmentation of node number results in the decrement of error. However, Cubic NEM behaves like a fine mesh method in 2-group examples. Besides slow convergence, error is decreasing sharply with respect to the increment of the node number, and it gets best results in terms of error versus its rivals after the node number reaches the saturation level.

3. DERECE NODAL AÇILIM METODUNUN SİLİNDİR GEOMETRİDE NÖTRON DİFÜZYON DENKLEMİNİN RADYAL BİLEŞKESİNE UYGULANMASI

ÖZET

Nükleer reaktörlerde kalp hesapları 2 temel teori üzerine dayanır: difüzyon ve transport teorisi. Transport denklemi konum, zaman, açı ve enerjiye bağlı olarak detaylı bir tasvir vermekle beraber kaba hesaplamalar için oldukça karmaşıktır. Difüzyon ise bu teoriye bir yaklaşım olup, transport ile kıyaslandığında çözümü daha kolaydır, bu sebeple de kaba hesaplamalar için daha pratiktir. Reaktor fiziğinde, enerji spektrumu göz önüne alındığında, stratejik olarak nötronların kalp içinde sahip oldukları enerji birden fazla gruba ayrılabilir. Bu nedenle çok gruplu nötron difüzyon denklemi kullanılır.

Günümüzde çok gruplu nötron difüzyon denklemi için bir çok farklı yöntem geliştirilmiştir. Bu yöntemler analitik, nümerik ve yarı-analitik olarak sınıflandırılır.

Nükleer mühendisliğin gelişimine bakıldığında, 70 yıllara kadar en çok kullanılan nümerik yöntemlerin başında FDM ve FEM geliyordu. Bu iki yöntemin ortak yanı zamanın bilgisayar özelliklerine uyumlu olmayıp oldukça yüksek belleklere gereksinim duymasıydı. Özellikle FDM iyi bir ızgaralandırma ve yoğun bir hücre yapısına ihtiyacı olduğu için bellek konusunda oldukça pahalı bir yöntem olarak göze çarpıyordu.

70lerden itibaren Nodal Yöntemler nükleer mühendislikte yerini alıp her 3 matematiksel yöntem grubunda da başarılı sonuçlarıyla göze çarptı. NEM olarak adlandırılan nümerik nodal yöntemler kaba ızgara yöntemi karakteristiği gösterdiğinden rakipleri olan FDM ve FEM göre çok daha kullanışlı idi. Binlerle ya da milyonlarla ifade edilen FDM sistemlerine göre, nodal yöntemlerin yaklaşık olarak FDM hücrelerinin 20 katı büyüklüğündeki nodları ve FEM'e göre de bellekte daha az yer kaplaması onun reaktor kalp hesaplarında son 35 yılın en popüler yöntemi olmasına sebep olmuştur.

NEM bir nümerik polinom açılım yöntemidir. Kullanılan polinomların derecesine göre düşük ($n=2$) ve yüksek dereceli ($n \geq 3$) olarak 2'ye ayrılabilir. Düşük açılımlar için Fick yasası ve nötron denge denklemi sistemi çözmek için yeterlidir. Ancak yüksek dereceli açılımlar için neutron akısının momentine ihtiyaç duyulur. Her n dereceli açılım, $n+1$ adet polinom ve açılım katsayısı gerektirir. Yüksek dereceli açılımlarda $n-2$ adet nötron akı momentini hesaplanır ve ağırlaştırılmış kalıntılar yöntemi $n-2$ defa uygulanır.

Bu çalışmada 3. Derece NEM yöntemi silindir geometride nötron difüzyon denkleminin radyal bileşkesine uygulanmıştır. Sistem oluşturulduktan sonra kodlama gerçekleştirilerek sistemin çözümleri elde edilmiştir. Yazılmış olan CNEMR kodu etkin nötron çoğaltma katsayısını, nodlar içindeki ortalama akıları ve bunlardan oluşan ortalama akıyı hesaplayabilmektedir. Bulunan sonuçlar 2. Derece NEM, Lineer FEM ve Kuadratik FEM sonuçlarıyla karşılaştırılmıştır.

Bulgular ışığında gözükür ki, 3. Derece Nodal Açılım Yöntemi tek gruplu problemlerde rakiplerine göre daha hızlı kabul edilebilir hata kriterine ulaşmaktadır. Gene tek gruplu problemlerde, nod sayısının arttırımı hata değerlerinde yavaş da olsa olumlu sonuçlar vermiştir. 2 gruplu problemlerde ise, düşük nod sayılarında beklenenden kötü bir performans çizmekte ama ilerleyen nod sayılarında hata değerlerinde keskin bir düşüş yaşanmaktadır. Nod sayısı belirli bir doygunluğa eriştikten sonra rakiplerinden daha iyi hata değerlerine ulaşmıştır.

1 INTRODUCTION

1.1 Diffusion Approximation

The principles of neutron dynamics have been related to the gas dynamics for a long time. Full physical description is maintained by neutron transport equation, which is based on Transport Equation derived by Boltzmann [1]. However, a steady state neutron transport equation is an integro-differential equation and may be considered as complicated for “coarse calculations” of nuclear reactors.

The steady state neutron transport equation is as follows:

$$\hat{\Omega} \cdot \nabla \phi(r, E, \hat{\Omega}) + \Sigma_t(r, E, \hat{\Omega}) \phi(r, E, \hat{\Omega}) = \int_{4\pi} d\hat{\Omega}' \int_0^{\infty} dE' \Sigma_s(r, E' \rightarrow E, \hat{\Omega}' \rightarrow \hat{\Omega}) \phi(r, E', \hat{\Omega}') + Q(r, E, \hat{\Omega}) \quad (1.1)$$

where,

- $\hat{\Omega}$ = Unit vector in direction of motion,
- $\phi(r, E, \hat{\Omega})$ = Angular flux,
- $\phi(r, E, \hat{\Omega}) dr dE d\hat{\Omega}$ = Number of neutrons in a differential volume dr about r , with a differential energy in dE about E , moving in a differential solid angle in $d\hat{\Omega}$ about $\hat{\Omega}$,
- $\Sigma_t(r, E, \hat{\Omega})$ = Macroscopic total cross section,
- $\Sigma_s(r, E' \rightarrow E, \hat{\Omega}' \rightarrow \hat{\Omega}) d\hat{\Omega}' dE'$ = Characterizes scattering of a neutron from an incident energy E and direction $\hat{\Omega}$ to a final energy E' in dE' and direction $\hat{\Omega}'$ in $d\hat{\Omega}'$,
- $Q(r, E, \hat{\Omega})$ = Source.

At this point, transport equation can be approximated to Neutron Diffusion equation for practical reactor core calculations. The overall effect of neutrons' collisions is that the neutrons undergo a kind of diffusion in the reactor medium, much like the diffusion of one gas in another. It is much simpler than the transport equation, because it removes the neutron direction of motion from consideration; the dependent variable is the total flux at each energy rather than the angular flux.

In order to derive the diffusion neutron diffusion equation, one-speed neutrons with isotropic collisions can be taken as the simplest example. First of all, the neutron current should be defined as ingoing and outgoing partial currents for each direction. Imagine a pure scattering medium, and let's focus on z-dependent neutron movement, then

$$J_z = j_z^+ - j_z^- \quad (1.2)$$

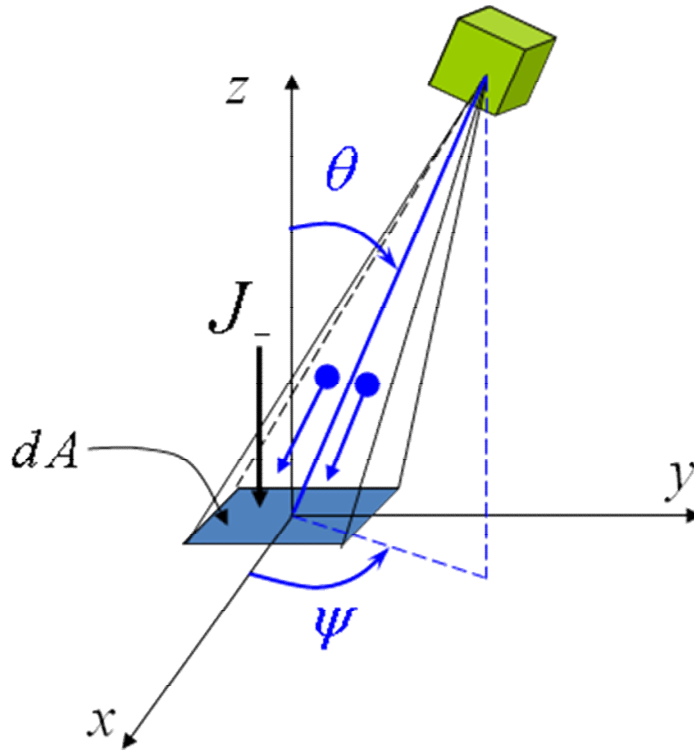


Figure 1.1 Geometry for derivation

Using geometrical properties, one can show that

$$j_z^- = \frac{\Sigma_s}{4\pi} \int_{\Psi=0}^{2\pi} \int_{\theta=0}^{\frac{\pi}{2}} \int_{r=0}^{\infty} \phi(r) \cos\theta e^{-\Sigma_s r} \sin\theta dr d\theta d\Psi \quad (1.3)$$

Taylor Expansion of the flux at origin results in:

$$\phi = \phi_0 + x \left(\frac{\partial\phi}{\partial x} \right)_{x=0} + y \left(\frac{\partial\phi}{\partial y} \right)_{y=0} + z \left(\frac{\partial\phi}{\partial z} \right)_{z=0} + \dots \quad (1.4)$$

If spherical coordinate transformation is applied

$$x = r \sin \theta \cos \Psi, \quad y = r \sin \theta \sin \Psi, \quad z = r \cos \theta. \quad (1.5)$$

Then (1.4) becomes

$$\phi(r) = \phi_0 + r \sin \theta \cos \Psi \left(\frac{\partial \phi}{\partial x} \right)_{x=0} + r \sin \theta \sin \Psi \left(\frac{\partial \phi}{\partial y} \right)_{y=0} + r \cos \theta \left(\frac{\partial \phi}{\partial z} \right)_{z=0} \quad (1.6)$$

Now, for just z-dependent ingoing partial current, putting (1.6) into (1.3) gives

$$\dot{j}_z = \frac{\Sigma_s}{4\pi} \int_{\Psi=0}^{2\pi} \int_{\theta=0}^{\frac{\pi}{2}} \int_{r=0}^{\infty} \left[\phi_0 + r \cos \theta \left(\frac{\partial \phi}{\partial z} \right)_{z=0} \right] e^{-\Sigma_s r} \cos \theta \sin \theta dr d\theta d\Psi \quad (1.7)$$

Because the terms containing $\cos \Psi$ and $\sin \Psi$ become zero when integrated over $0 \leq \Psi \leq 2\pi$.

Thus,

$$\dot{j}_z = \frac{\phi_0}{4} + \frac{1}{6\Sigma_s} \left(\frac{\partial \phi}{\partial z} \right)_{z=0} \quad (1.8)$$

Using (1.2)

$$J_z = -\frac{1}{3\Sigma_s} \left(\frac{\partial \phi}{\partial z} \right)_{z=0} \quad (1.9)$$

Similarly,

$$J_x = -\frac{1}{3\Sigma_s} \left(\frac{\partial \phi}{\partial x} \right)_{x=0} \quad \text{and} \quad J_y = -\frac{1}{3\Sigma_s} \left(\frac{\partial \phi}{\partial y} \right)_{y=0} \quad (1.10)$$

By the way, the general vector form of neutron current is

$$\vec{J} = -\frac{1}{3\Sigma_s} \underbrace{\left(e_x \frac{\partial \phi}{\partial x} + e_y \frac{\partial \phi}{\partial y} + e_z \frac{\partial \phi}{\partial z} \right)}_{\nabla \phi} \quad (1.11)$$

Assume that $D = \frac{1}{3\Sigma_s}$ in Lab system, we finally arrive to Fick's law: $\vec{J} = -D \vec{\nabla} \phi$

Here, some general properties can be revealed:

- Flux is finite, real and non-negative
- Flux preserves the symmetry

- Flux and current are continuous

The diffusion equation is ready to be derived after the relation between the neutron current and neutron flux is shown.

Consider an arbitrary volume V and establish the following balance:

$$\left[\begin{array}{l} \text{rate of change} \\ \text{of the number of} \\ \text{neutrons in } V \end{array} \right] = \left[\begin{array}{l} \text{rate of production} \\ \text{of neutrons in } V \end{array} \right] - \left[\begin{array}{l} \text{rate of absorption} \\ \text{of neutrons in } V \end{array} \right] - \left[\begin{array}{l} \text{rate of leakage} \\ \text{of neutrons from } V \end{array} \right] \quad (1.12)$$

Then,

$$\left[\begin{array}{l} \text{rate of change} \\ \text{of the number of} \\ \text{neutrons in } V \end{array} \right] = \frac{d}{dt} \int_V N(\mathbf{r}, t) dV, \quad (1.13)$$

$$\left[\begin{array}{l} \text{rate of production} \\ \text{of neutrons in } V \end{array} \right] = \int_V Q(\mathbf{r}, t) dV, \quad (1.14)$$

$$\left[\begin{array}{l} \text{rate of absorption} \\ \text{of neutrons in } V \end{array} \right] = \int_V \Sigma_a \phi(\mathbf{r}, t) dV \quad (1.15)$$

$$\left[\begin{array}{l} \text{rate of leakage} \\ \text{of neutrons from } V \end{array} \right] = \int_S \vec{J} \cdot \hat{n} dS = \int_V \vec{\nabla} \cdot \vec{J}(\mathbf{r}, t) dV. \quad (1.16)$$

If one writes down the time dependent balance equation:

$$\frac{d}{dt} \int_V N(\mathbf{r}, t) dV = \int_V Q(\mathbf{r}, t) dV - \int_V \Sigma_a \phi(\mathbf{r}, t) dV - \int_V \vec{\nabla} \cdot \vec{J}(\mathbf{r}, t) dV \quad (1.17)$$

The next step is to remove the integration from both sides of the equations:

$$\frac{dN(\mathbf{r}, t)}{dt} = Q(\mathbf{r}, t) - \Sigma_a \phi(\mathbf{r}, t) - \vec{\nabla} \cdot \vec{J}(\mathbf{r}, t) \quad (1.18)$$

Finally, in order to get the steady state neutron diffusion equation, time dependency should be vanished, and if the Fick's law is applied:

$$-D\nabla^2 \phi(\mathbf{r}) + \Sigma_a \phi(\mathbf{r}) = Q(\mathbf{r}) \quad (1.19)$$

It should be emphasized that neutron diffusion equation is an approximation, and it requires assumptions for its validity.

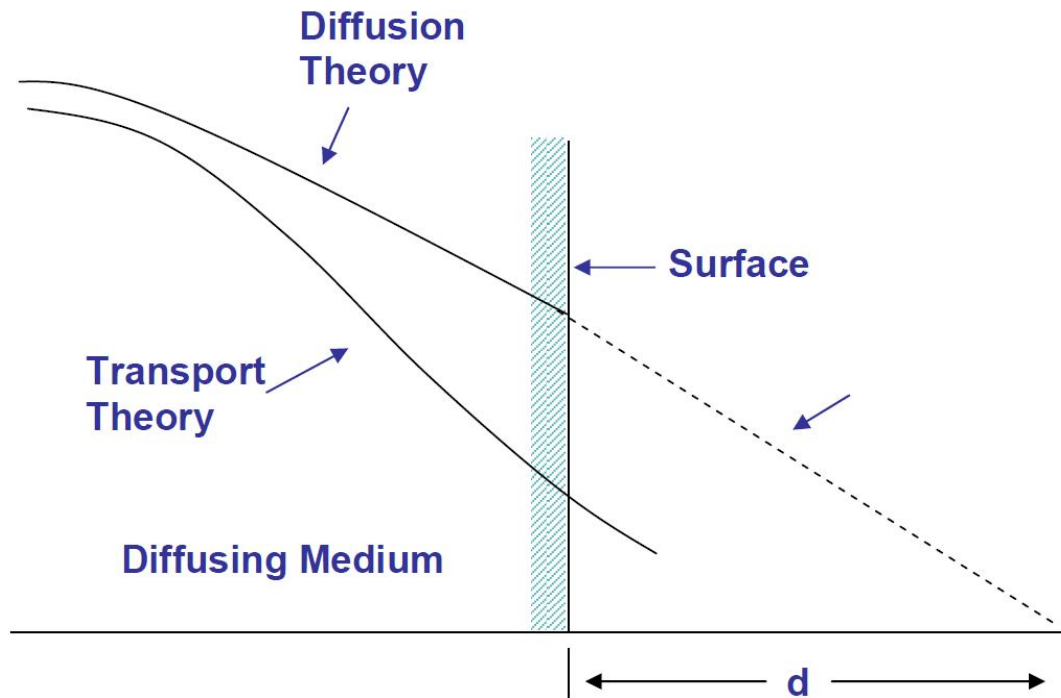


Figure 1.2 Extrapolation Distance

Here, d is the extrapolation distance [2], and it is equal to $0.71 \lambda_{tr}$ which is the transport mean free path (cm). The general approximated relation between the diffusion constant and transport mean free path is:

$$D = \frac{1}{3\Sigma_{tr}} = 3\lambda_{tr} \quad (1.20)$$

In short, a steady state diffusion theory is invalid under these conditions [2]:

- in a medium that strongly absorbs neutrons,
- within three mean free paths of either a neutron source or the surface of a material,
- when neutron scattering is strongly anisotropic.

1.2 Nodal Expansion Method

History of the nuclear engineering signifies that FDM and FEM [3,4] had been the most popular numerical methods which were employed for core calculations till 70s. The common point of these two methods was the inconvenience to the computer configurations of the period due to high computer memory requirement. Especially, FDM is not practical for accurate solutions of core problems because of its high cost.

Spatial cell sizes may reduce the computer time; however, FDM becomes inaccurate. Nodal methods [5,6] have been popular since 70s, due to their advantage in increasing the speed of the computations, and their coarse mesh compared to fine mesh finite difference solutions [7]. The nodal methods divide the reactor core into large regions named “nodes” and represent the flux distribution averaging inside nodes. Probably, the most common popular nodal methods are transverse integrated nodal methods [5]. In this class of nodal methods the three-dimensional multigroup neutron diffusion equation is replaced by three ODEs. These one dimensional equations are obtained by integrating the 3-D neutron diffusion equation over the two directions transverse to aimed direction.

Among the various polynomial methods, the Nodal Expansion Method (NEM) developed by Finnemann and Bennewitz [8] is situated to an important place in nodal diffusion calculations. NEM, one of the earliest polynomial methods, originated from the Nodal Synthesis Method [9]. Higher order expansions can be also performed [8]. Three of the coefficients of these polynomials are calculated by demanding neutron balance [7] for each node, and continuity of the surface average fluxes and currents between two adjacent nodes [10]. For high order cases, the remaining coefficients are determined by using preservation of higher moments of the flux using a weighted residual technique [11] on the transverse integrated diffusion equation.

1.3 Objectives of the Work

The objective of this study is to derive the system formed by Cubic NEM, and to compare the results with other methods in order to expose the performance. Cubic NEM is applied to neutron diffusion equation for radial solution in cylindrical geometry. The main comparison is made between Quadratic NEM and Cubic NEM to understand the difference. CNEMR, code built in FORTRAN, is able to perform both Quadratic and Cubic NEM.

For a short description, Chapter 2 begins with the group independent derivation of the system which formed by Fick’s law, neutron balance, and first moment of neutron diffusion equation. Then, the system obtained is reformulated under group dependency.

In Chapter 3, 4 numerical applications are shown. Analytical solutions are made for three of them; Quadratic FEM with 320 elements is taken as reference in the

remaining one. Effective neutron multiplication constants and neutron fluxes obtained from CNEMR and QFEMR are compared. The comparisons are based on convergence to a certain error percentage, coarse mesh performance, and response towards refinement.

2 NODAL FORMALISM IN CYLINDRICAL GEOMETRY

2.1 Node Averaged Quantities and Moments

Assuming that

- All collisions are isotropic,
- Axial component is so long($z \gg r$), so there is no leakage from this direction,

Then, the multigroup neutron balance equation

$$\vec{\nabla} \cdot \vec{J}_g(\vec{r}) + \Sigma_r^g(\vec{r})\phi_g(\vec{r}) = \sum_{g'=1}^{g-1} \Sigma^{g' \rightarrow g}(\vec{r})\phi_{g'}(\vec{r}) + \frac{\chi^g}{k} \sum_{g'=1}^G \nu \Sigma_f^{g'}(\vec{r})\phi_{g'}(\vec{r}), \quad g = 1, 2, \dots, G \quad (2.1)$$

with no group-to-group upscatter assumption, and Fick's Law

$$\vec{J}_g(\vec{r}) = -D^g(\vec{r})\vec{\nabla}\phi_g(\vec{r}) \quad (2.2)$$

constitutes the basis of the nodal formalism.

To avoid complexity in notation, scattering and fission sources will be defined as

$$Q_g(\vec{r}) = \sum_{g'=1}^{g-1} \Sigma^{g' \rightarrow g}(\vec{r})\phi_{g'}(\vec{r}) + \frac{\chi^g}{k} \sum_{g'=1}^G \nu \Sigma_f^{g'}(\vec{r})\phi_{g'}(\vec{r}), \quad g = 1, 2, \dots, G \quad (2.3)$$

Thus, (2.1) becomes

$$\vec{\nabla} \cdot \vec{J}_g(\vec{r}) + \Sigma_r^g(\vec{r})\phi_g(\vec{r}) = Q_g(\vec{r}) \quad (2.4)$$

Since group index is of no immediate concern in nodal development, the group indices will be suppressed and (2.4) and (2.2) will be written as

$$\vec{\nabla} \cdot \vec{J}(\vec{r}) + \Sigma_r(\vec{r})\phi(\vec{r}) = Q(\vec{r}) \quad (2.5)$$

$$\vec{J}(\vec{r}) = -D(\vec{r})\vec{\nabla}\phi(\vec{r}) \quad (2.6)$$

Figure 2.1 illustrates a cylindrical mesh having nodes $A_i=(r_{i-1/2}, r_{i+1/2})$. The radii at node centers are similarly denoted as (r_i) and it is convenient to define mesh spacing $\Delta r_i=r_{i+1/2}-r_{i-1/2}$.

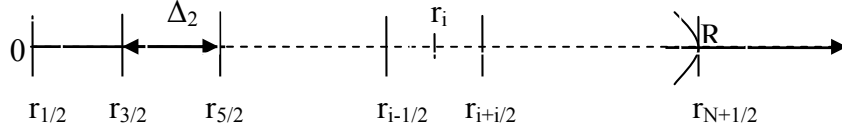


Figure 2.1 Nodal Mesh Imposed on One-dimensional Cylindrical Domain

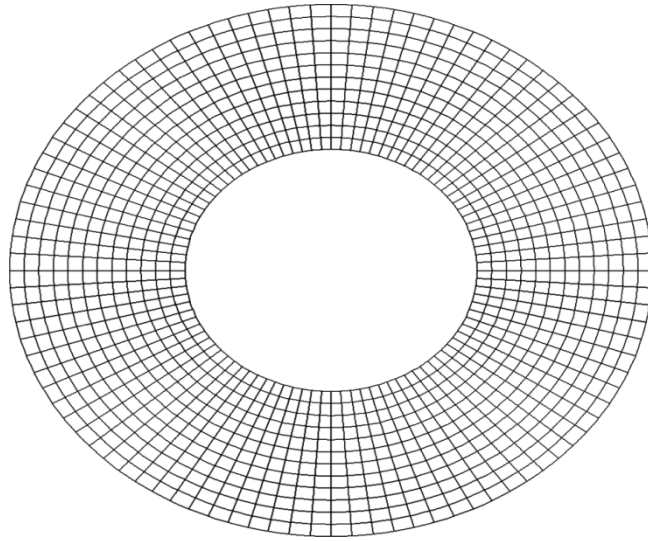


Figure 2.2 Multigrid of Radial Component in Cylindrical Domain

Δr_i is replaced with Δ_i for simplicity

$$\Delta_i = r_{i+1/2} - r_{i-1/2} \quad (2.7)$$

Inherited from the nodal perspective and common to all nodal discretizations is the choice of node and edge-based unknowns. The node-based unknowns are defined by

$$\phi_i = \frac{2}{(r_{i+1/2}^2 - r_{i-1/2}^2)} \int_{r_{i-1/2}}^{r_{i+1/2}} \phi(r) r dr \quad (2.8)$$

$$Q_i = \frac{2}{(r_{i+1/2}^2 - r_{i-1/2}^2)} \int_{r_{i-1/2}}^{r_{i+1/2}} Q(r) r dr \quad (2.9)$$

$$\phi_{i,n} = \frac{2}{(r_{i+1/2}^2 - r_{i-1/2}^2)} \int_{r_{i-1/2}}^{r_{i+1/2}} w_n \phi(r) r dr \quad (2.10)$$

where w_n is the weight function of n^{th} order.

These terms are the node average flux, source, and the moment of neutron flux respectively. While the edged-based unknowns, namely edge average fluxes and currents are just point fluxes and currents at node boundaries in one dimension, because there is no other dimension over which to find averages. They are shown as $\phi_{i+1/2}$, $\phi_{i-1/2}$ and $J_{i+1/2}$, $J_{i-1/2}$

In some nodal methods, edge-averaged partial currents are also needed. To avoid notational complexity, the partial currents will be denoted by the lower case letter j . $j_{i+1/2}^+$ and $j_{i-1/2}^-$ denote the outgoing partial currents, while $j_{i+1/2}^-$ and $j_{i-1/2}^+$ are the incoming partial currents at the right ($i+1/2$) and left ($i-1/2$) edges respectively.

Under P_1 approximation [12]

$$j_u^\pm(\mathbf{r}) = \frac{\phi(\mathbf{r})}{4} \pm \frac{\vec{n}_u \cdot \vec{J}(\mathbf{r})}{2} \quad (2.11)$$

where u is an arbitrary direction.

If diffusion theory is valid,

$$j_u^\pm(\mathbf{r}) = \frac{1}{4} \phi(\mathbf{r}) \mp \frac{D(\mathbf{r})}{2} \frac{\partial \phi(\mathbf{r})}{\partial r} \quad (2.12)$$

from (2.10), obviously:

$$J_{i+1/2} = j_{i+1/2}^+ - j_{i+1/2}^- \quad (2.13)$$

$$J_{i-1/2} = j_{i-1/2}^+ - j_{i-1/2}^- \quad (2.14)$$

and

$$\phi_{i+1/2} = 2(j_{i+1/2}^+ + j_{i+1/2}^-) \quad (2.15)$$

$$\phi_{i-1/2} = 2(j_{i-1/2}^+ + j_{i-1/2}^-) \quad (2.16)$$

2.2 Cubic Nodal Expansion Method

2.2.1 Construction of Polynomial Basis

The NEM treatment of the transverse integrated ODE's is based on a third order polynomial expansion of the transverse integrated flux. In one dimension this is just r dependent flux

$$\phi(r) = \sum_{n=0}^3 a_n P_n(r), \quad r_{i-1/2} < r < r_{i+1/2} \quad (2.17)$$

At this point a normalized variable ξ is defined as

$$\xi = \frac{r - r_i}{\Delta_i} \quad (2.18)$$

where $\xi = \pm 1/2$ when $r = r_{i \pm 1/2}$.

ξ and r are the same order. Then, (2.17) can be written in normalized variable

$$\phi(\xi) = \sum_{n=0}^3 a_n P_n(\xi), \quad -1/2 < \xi < 1/2 \quad (2.19)$$

where $P_n(\xi)$ is a polynomial of degree n .

For simplicity, the first polynomial is chosen as

$$P_0(\xi) = 1 \quad (2.20)$$

and the higher order polynomials are required to be orthogonal to $P_0(\xi)$

$$\int_{-1/2}^{1/2} P_n(\xi) d\xi = 0, \quad n \neq 0 \quad (2.21)$$

Transformation of integration operator gives

$$d\xi = \frac{dr}{\Delta_i} \quad (2.22)$$

The node averaged flux is

$$\phi_i = \frac{2}{(r_{i+1/2}^2 - r_{i-1/2}^2)} \int_{-1/2}^{1/2} \phi(\xi) (\xi \Delta_i + r_i) \Delta_i d\xi \quad (2.23)$$

Simplification gives

$$\phi_i = \frac{1}{\Delta_i r_i} \int_{-1/2}^{1/2} \phi(\xi) (\xi \Delta_i + r_i) \Delta_i d\xi \quad (2.24)$$

Inserting (2.19) into (2.24)

$$\phi_i = \frac{1}{\Delta_i r_i} \int_{-1/2}^{1/2} \left(\sum_{n=0}^3 a_n P_n(\xi) \right) (\xi \Delta_i + r_i) \Delta_i d\xi \quad (2.25)$$

Thus,

$$\phi_i = \frac{1}{r_i} \int_{-1/2}^{1/2} (a_0 P_0(\xi) + a_1 P_1(\xi) + a_2 P_2(\xi) + a_3 P_3(\xi)) (\xi \Delta_i + r_i) d\xi \quad (2.26)$$

Due to the orthogonality,

$$\int_{-1/2}^{1/2} (a_1 P_1(\xi) + a_2 P_2(\xi) + a_3 P_3(\xi)) d\xi = 0 \quad \text{and} \quad \int_{-1/2}^{1/2} a_0 P_0(\xi) \xi \Delta_i d\xi = 0 \quad (2.27)$$

Finally,

$$\phi_i = \frac{1}{r_i} \int_{-1/2}^{1/2} (a_0 r_i P_0(\xi) + a_1 P_1(\xi) \xi \Delta_i + a_2 P_2(\xi) \xi \Delta_i + a_3 P_3(\xi) \xi \Delta_i) d\xi \quad (2.28)$$

One can derive the following polynomials by using the orthogonality identity and putting convenient values into arbitrary constants [13]:

$$P_1(\xi) = \xi \quad (2.29)$$

$$P_2(\xi) = 3\xi^2 - \frac{1}{4} \quad (2.30)$$

$$P_3(\xi) = \xi \left(\xi - \frac{1}{2} \right) \left(\xi + \frac{1}{2} \right) \quad (2.31)$$

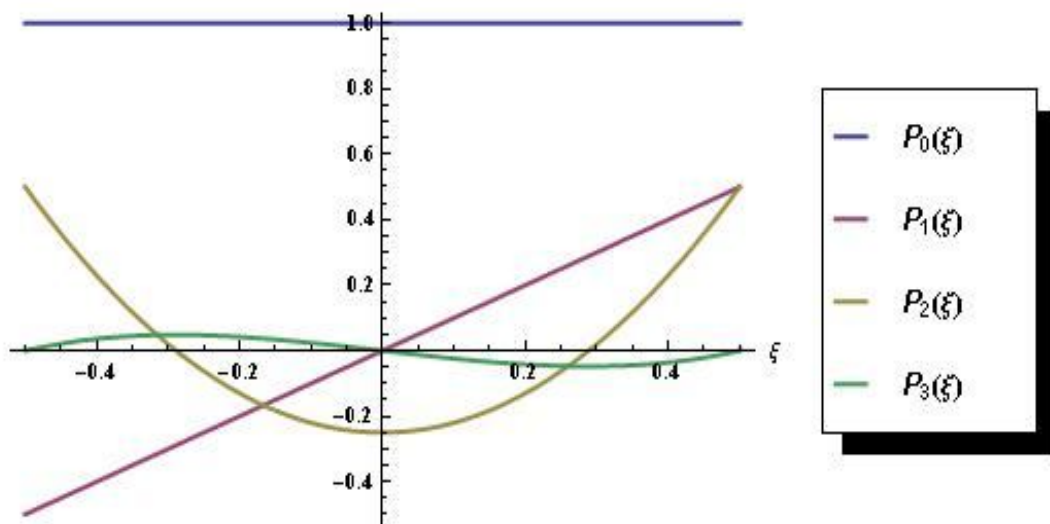


Figure 2.3 The Basis Polynomials

2.2.2 Determination of Expansion Coefficients

Recall the equation (2.26)

$$\phi_i = \frac{1}{r_i} \int_{-1/2}^{1/2} (a_0 r_i P_0(\xi) + a_1 P_1(\xi) \xi \Delta_i + a_2 P_2(\xi) \xi \Delta_i + a_3 P_3(\xi) \xi \Delta_i) d\xi$$

Then,

$$a_0 \int_{-1/2}^{1/2} P_0(\xi) d\xi = a_0 \quad (2.32)$$

$$\frac{a_1 \Delta_i}{r_i} \int_{-1/2}^{1/2} P_1(\xi) \xi d\xi = \frac{a_1 \Delta_i}{12 r_i} \quad (2.33)$$

$$\frac{a_2 \Delta_i}{r_i} \int_{-1/2}^{1/2} P_2(\xi) \xi d\xi = 0 \quad (2.34)$$

$$\frac{a_3 \Delta_i}{r_i} \int_{-1/2}^{1/2} P_3(\xi) \xi d\xi = -\frac{a_3 \Delta_i}{120 r_i} \quad (2.35)$$

Finally,

$$\phi_i = a_0 + \frac{a_1 \Delta_i}{12 r_i} - \frac{a_3 \Delta_i}{120 r_i} \quad (2.36)$$

Now, starting and end points of a node should be defined in terms of expansion coefficients. Moreover, high order polynomials are restricted ($n > 2$), which means:

$$P_3\left(\pm \frac{1}{2}\right) = 0 \quad (2.37)$$

Then,

$$\phi_{i+\frac{1}{2}} = \sum_{n=0}^3 a_n P_n\left(\frac{1}{2}\right) = a_0 P_0\left(\frac{1}{2}\right) + a_1 P_1\left(\frac{1}{2}\right) + a_2 P_2\left(\frac{1}{2}\right) + a_3 P_3\left(\frac{1}{2}\right) \quad (2.38)$$

$$\phi_{i+\frac{1}{2}} = a_0 + \frac{a_1}{2} + \frac{a_2}{2} \quad (2.39)$$

and

$$\phi_{i-\frac{1}{2}} = \sum_{n=0}^3 a_n P_n\left(-\frac{1}{2}\right) = a_0 P_0\left(-\frac{1}{2}\right) + a_1 P_1\left(-\frac{1}{2}\right) + a_2 P_2\left(-\frac{1}{2}\right) + a_3 P_3\left(-\frac{1}{2}\right) \quad (2.40)$$

$$\phi_{i-\frac{1}{2}} = a_0 - \frac{a_1}{2} + \frac{a_2}{2} \quad (2.41)$$

Till this point, 3 equations are obtained from node points. However, 3 equations are not sufficient to find 4 expansion coefficients. By the way, high order expansions require supplementary terms which are called as moments. An n^{th} order expansion needs to have $n-2$ moment(s) to get solved. So, just first moment of neutron flux is enough for cubic expansion in order to establish a system.

Remember that n^{th} moment of neutron flux was $\phi_{i,n} = \frac{2}{(r_{i+1/2}^2 - r_{i-1/2}^2)} \int_{r_{i-1/2}}^{r_{i+1/2}} w_n \phi(r) r dr$. By

the way, first moment of neutron will be following term:

$$\phi_{i,1} = \frac{2}{(r_{i+1/2}^2 - r_{i-1/2}^2)} \int_{r_{i-1/2}}^{r_{i+1/2}} w_1 \phi(r) r dr \quad (2.42)$$

Here, the weight function w_1 is equivalent to the first order polynomial P_1 . Hence,

$$\phi_{i,1} = \frac{1}{\Delta_i r_{i-1/2}} \int_{r_{i-1/2}}^{r_{i+1/2}} P_1(\xi) \phi(\xi) (\xi \Delta_i + r_i) \Delta_i d\xi = \frac{1}{\Delta_i r_{i-1/2}} \int_{-1/2}^{1/2} \xi \left(\sum_{n=0}^3 a_n P_n(\xi) \right) (\xi \Delta_i + r_i) \Delta_i d\xi \quad (2.43)$$

After the evaluation of the integral, the moment of neutron flux can be written as follows:

$$\phi_{i,1} = \frac{a_0 \Delta_i}{12 r_i} + \frac{a_1}{12} + \frac{a_2 \Delta_i}{60 r_i} - \frac{a_3}{120} \quad (2.44)$$

$$\begin{bmatrix} 1 & \frac{\Delta_i}{12 r_i} & 0 & -\frac{\Delta_i}{120 r_i} \\ 1 & \frac{1}{2} & \frac{1}{2} & 0 \\ 1 & -\frac{1}{2} & \frac{1}{2} & 0 \\ \frac{\Delta_i}{12 r_i} & \frac{1}{12} & \frac{\Delta_i}{60 r_i} & -\frac{1}{120} \end{bmatrix} \begin{bmatrix} a_0 \\ a_1 \\ a_2 \\ a_3 \end{bmatrix} = \begin{bmatrix} \phi_i \\ \phi_{i+\frac{1}{2}} \\ \phi_{i-\frac{1}{2}} \\ \phi_{i,1} \end{bmatrix} \quad (2.45)$$

After the solution of the linear system above, the expansion coefficients are revealed:

$$\text{Let } \alpha_i = \frac{5}{\left[1 - 20 \left(\frac{r_i}{\Delta_i} \right)^2 \right]} \quad (2.46)$$

Then,

$$a_0 = \frac{\alpha_i}{15} \left[-\phi_{i+\frac{1}{2}} - \phi_{i-\frac{1}{2}} + 60\phi_{i,1} \left(\frac{r_i}{\Delta_i} \right) - 60\phi_i \left(\frac{r_i}{\Delta_i} \right)^2 \right] \quad (2.47)$$

$$a_1 = \phi_{i+\frac{1}{2}} - \phi_{i-\frac{1}{2}} \quad (2.48)$$

$$a_2 = \frac{\alpha_i}{3} \left[\phi_{i+\frac{1}{2}} \left[1 - 12 \left(\frac{r_i}{\Delta_i} \right)^2 \right] + \phi_{i-\frac{1}{2}} \left[1 - 12 \left(\frac{r_i}{\Delta_i} \right)^2 \right] - 24\phi_{i,1} \left(\frac{r_i}{\Delta_i} \right) + 24\phi_i \left(\frac{r_i}{\Delta_i} \right)^2 \right] \quad (2.49)$$

$$a_3 = 2\alpha_i \left[\phi_{i+\frac{1}{2}} \left[1 - 4 \left(\frac{r_i}{\Delta_i} \right) - 20 \left(\frac{r_i}{\Delta_i} \right)^2 \right] - \phi_{i-\frac{1}{2}} \left[1 + 4 \left(\frac{r_i}{\Delta_i} \right) - 20 \left(\frac{r_i}{\Delta_i} \right)^2 \right] \right] \quad (2.50)$$

$$+ 2\alpha_i \left[-12\phi_i \left(\frac{r_i}{\Delta_i} \right) + 240\phi_{i,1} \left(\frac{r_i}{\Delta_i} \right)^2 \right]$$

2.3 Fick's Law

Fick's law states that

$$J(r) = -D \frac{d\phi(r)}{dr} \quad (2.51)$$

Note that

$$\frac{d\phi(r)}{dr} = \frac{d\phi}{d\xi} \frac{d\xi}{dr} = \frac{1}{\Delta_i} \frac{d\phi(\xi)}{d\xi} \quad (2.52)$$

(2.50) may be written as

$$J(\xi) = -\frac{D_i}{\Delta_i} \frac{d\phi(\xi)}{d\xi} \quad (2.53)$$

Using (2.19)

$$\frac{d\phi(\xi)}{d\xi} = a_0 \frac{dP_0}{d\xi} + a_1 \frac{dP_1}{d\xi} + a_2 \frac{dP_2}{d\xi} + a_3 \frac{dP_3}{d\xi} \quad (2.54)$$

Then,

$$J(\xi) = -\frac{D_i}{\Delta_i} \left[a_1 + a_2 6\xi + a_3 \left(3\xi^2 - \frac{1}{4} \right) \right] \quad (2.55)$$

for $\xi=+1/2$

$$J\left(\frac{1}{2}\right) = J_{i+1/2} = -\frac{D_i}{\Delta_i} \left[a_1 + 3a_2 + \frac{a_3}{2} \right] \quad (2.56)$$

Similarly, for $\xi=-1/2$

$$J\left(-\frac{1}{2}\right) = J_{i-1/2} = -\frac{D_i}{\Delta_i} \left[a_1 - 3a_2 + \frac{a_3}{2} \right] \quad (2.57)$$

Now, put the expansion coefficients into current terms:

$$\text{Let } \theta_i = -\frac{D_i}{\Delta_i} \quad (2.58)$$

Starting with $J_{i+1/2}$,

$$\begin{aligned} J_{i+1/2} = & \theta_i \left[\left(\phi_{i+1/2} - \phi_{i-1/2} \right) + \alpha_i \left[\phi_{i+1/2} \left[2 - 32 \left(\frac{r_i}{\Delta_i} \right)^2 - 4 \left(\frac{r_i}{\Delta_i} \right) \right] \right] \right] \\ & + \theta_i \alpha_i \left[\phi_{i-1/2} \left[8 \left(\frac{r_i}{\Delta_i} \right)^2 - 4 \left(\frac{r_i}{\Delta_i} \right) \right] + \phi_i \left[24 \left(\frac{r_i}{\Delta_i} \right)^2 - 12 \left(\frac{r_i}{\Delta_i} \right) \right] \right] \\ & + \theta_i \alpha_i \left[\phi_{i,1} \left[240 \left(\frac{r_i}{\Delta_i} \right)^2 - 24 \left(\frac{r_i}{\Delta_i} \right) \right] \right] \end{aligned} \quad (2.59)$$

First, use (2.13) and (2.14) to expand the currents, then (2.15) and (2.16) to expand the flux in order to express them with ingoing and outgoing partial currents:

$$\begin{aligned} j_{i+1/2}^+ - j_{i+1/2}^- = & \theta_i \left[j_{i+1/2}^+ + j_{i+1/2}^- - j_{i-1/2}^+ - j_{i-1/2}^- \right] \\ & + \theta_i \alpha_i \left[2 \left(j_{i+1/2}^+ + j_{i+1/2}^- \right) \underbrace{\left[2 - 32 \left(\frac{r_i}{\Delta_i} \right)^2 - 4 \left(\frac{r_i}{\Delta_i} \right) \right]}_{A_i} \right] \\ & + \theta_i \alpha_i \left[2 \left(j_{i-1/2}^+ + j_{i-1/2}^- \right) \underbrace{\left[8 \left(\frac{r_i}{\Delta_i} \right)^2 - 4 \left(\frac{r_i}{\Delta_i} \right) \right]}_{B_i} + \phi_i \left[24 \left(\frac{r_i}{\Delta_i} \right)^2 - 12 \left(\frac{r_i}{\Delta_i} \right) \right] \right] \\ & + \theta_i \alpha_i \left[\phi_{i,1} \left[240 \left(\frac{r_i}{\Delta_i} \right)^2 - 24 \left(\frac{r_i}{\Delta_i} \right) \right] \right] \end{aligned} \quad (2.60)$$

After arrangements and factorizations, one can get following equation:

$$\begin{aligned}
j_{i+\frac{1}{2}}^+ &= \frac{(1+2\theta_i+2\theta_i\alpha_iA_i)}{(1-2\theta_i-2\theta_i\alpha_iA_i)}j_{i+\frac{1}{2}}^- + \frac{(2\theta_i\alpha_iB_i-2\theta_i)}{(1-2\theta_i-2\theta_i\alpha_iA_i)}j_{i-\frac{1}{2}}^- \\
&+ \frac{(2\theta_i\alpha_iB_i-2\theta_i)}{(1-2\theta_i-2\theta_i\alpha_iA_i)}j_{i-\frac{1}{2}}^+ \\
&+ \frac{\theta_i\alpha_i}{(1-2\theta_i-2\theta_i\alpha_iA_i)}\left[24\left(\frac{r_i}{\Delta_i}\right)^2-12\left(\frac{r_i}{\Delta_i}\right)\right]\phi_i \\
&+ \frac{\theta_i\alpha_i}{(1-2\theta_i-2\theta_i\alpha_iA_i)}\left[240\left(\frac{r_i}{\Delta_i}\right)^2-24\left(\frac{r_i}{\Delta_i}\right)\right]\phi_{i,1}
\end{aligned} \tag{2.61}$$

One can apply the same procedure for $J_{i-1/2}$ and obtain:

$$\begin{aligned}
j_{i-\frac{1}{2}}^- &= \frac{(2\theta_i\alpha_iE_i-2\theta_i-1)}{(2\theta_i-2\theta_i\alpha_iE_i-1)}j_{i-\frac{1}{2}}^+ + \frac{(2\theta_i-2\theta_i\alpha_iF_i)}{(2\theta_i-2\theta_i\alpha_iE_i-1)}j_{i+\frac{1}{2}}^+ + \frac{(2\theta_i-2\theta_i\alpha_iF_i)}{(2\theta_i-2\theta_i\alpha_iE_i-1)}j_{i+\frac{1}{2}}^- \\
&- \frac{\theta_i\alpha_i}{(2\theta_i-2\theta_i\alpha_iE_i-1)}\left[24\left(\frac{r_i}{\Delta_i}\right)^2+12\left(\frac{r_i}{\Delta_i}\right)\right]\phi_i \\
&+ \frac{\theta_i\alpha_i}{(2\theta_i-2\theta_i\alpha_iE_i-1)}\left[240\left(\frac{r_i}{\Delta_i}\right)^2+24\left(\frac{r_i}{\Delta_i}\right)\right]\phi_{i,1}
\end{aligned} \tag{2.62}$$

where

$$E_i = 32\left(\frac{r_i}{\Delta_i}\right)^2 - 4\left(\frac{r_i}{\Delta_i}\right) - 2 \tag{2.63}$$

and

$$F_i = 8\left(\frac{r_i}{\Delta_i}\right)^2 + 4\left(\frac{r_i}{\Delta_i}\right) \tag{2.64}$$

To avoid complexity in notation, more discretized terms may be defined. For the equation (2.61):

$$\frac{(1+2\theta_i+2\theta_i\alpha_iA_i)}{(1-2\theta_i-2\theta_i\alpha_iA_i)} = k_i \tag{2.65}$$

$$\frac{(2\theta_i\alpha_iB_i-2\theta_i)}{(1-2\theta_i-2\theta_i\alpha_iA_i)} = l_i \tag{2.66}$$

$$\frac{\theta_i \alpha_i}{(1 - 2\theta_i - 2\theta_i \alpha_i A_i)} = m_i \quad (2.67)$$

For the equation (2.62):

$$\frac{(2\theta_i \alpha_i E_i - 2\theta_i - 1)}{(2\theta_i - 2\theta_i \alpha_i E_i - 1)} = x_i \quad (2.68)$$

$$\frac{(2\theta_i - 2\theta_i \alpha_i F_i)}{(2\theta_i - 2\theta_i \alpha_i E_i - 1)} = y_i \quad (2.69)$$

$$\frac{\theta_i \alpha_i}{(2\theta_i - 2\theta_i \alpha_i E_i - 1)} = z_i \quad (2.70)$$

After these new defined discretized terms, the equations become:

$$\begin{aligned} j_{i+\frac{1}{2}}^+ &= k_i j_{i+\frac{1}{2}}^- + l_i j_{i-\frac{1}{2}}^- + l_i j_{i-\frac{1}{2}}^+ + m_i \left[24 \left(\frac{r_i}{\Delta_i} \right)^2 - 12 \left(\frac{r_i}{\Delta_i} \right) \right] \phi_i \\ &+ m_i \left[240 \left(\frac{r_i}{\Delta_i} \right)^2 - 24 \left(\frac{r_i}{\Delta_i} \right) \right] \phi_{i,1} \end{aligned} \quad (2.71)$$

and

$$\begin{aligned} j_{i-\frac{1}{2}}^- &= x_i j_{i-\frac{1}{2}}^+ + y_i j_{i+\frac{1}{2}}^+ + y_i j_{i+\frac{1}{2}}^- - z_i \left[24 \left(\frac{r_i}{\Delta_i} \right)^2 + 12 \left(\frac{r_i}{\Delta_i} \right) \right] \phi_i \\ &+ z_i \left[240 \left(\frac{r_i}{\Delta_i} \right)^2 + 24 \left(\frac{r_i}{\Delta_i} \right) \right] \phi_{i,1} \end{aligned} \quad (2.72)$$

(2.71) and (2.72) are the expressions for the outgoing partial currents. Substitute the outgoing current $j_{i-1/2}^-$ defined by (2.72) into (2.71), then simplify:

$$\begin{aligned} j_{i+\frac{1}{2}}^+ &= \left(\frac{k_i + l_i y_i}{1 - l_i y_i} \right) j_{i+\frac{1}{2}}^- + \left(\frac{l_i + l_i x_i}{1 - l_i y_i} \right) j_{i-\frac{1}{2}}^- \\ &+ \frac{12 \left[2(m_i - l_i z_i) \left(\frac{r_i}{\Delta_i} \right)^2 + (-l_i z_i - m_i) \left(\frac{r_i}{\Delta_i} \right) \right]}{(1 - l_i y_i)} \phi_i \\ &+ \frac{24 \left[10(m_i + l_i z_i) \left(\frac{r_i}{\Delta_i} \right)^2 + (l_i z_i - m_i) \left(\frac{r_i}{\Delta_i} \right) \right]}{(1 - l_i y_i)} \phi_{i,1} \end{aligned} \quad (2.73)$$

Similarly, substituting the outgoing current $j_{i+1/2}^+$ defined by (2.71) into (2.72), then simplify:

$$\begin{aligned}
j_{i-1/2}^- &= \left(\frac{x_i + l_i y_i}{1 - l_i y_i} \right) j_{i-1/2}^+ + \left(\frac{y_i + y_i k_i}{1 - l_i y_i} \right) j_{i+1/2}^- \\
&+ \frac{12 \left[2(y_i m_i - z_i) \left(\frac{r_i}{\Delta_i} \right)^2 + (-z_i - y_i m_i) \left(\frac{r_i}{\Delta_i} \right) \right]}{(1 - l_i y_i)} \phi_i \\
&+ \frac{24 \left[10(y_i m_i + z_i) \left(\frac{r_i}{\Delta_i} \right)^2 + (z_i - m_i y_i) \left(\frac{r_i}{\Delta_i} \right) \right]}{(1 - l_i y_i)} \phi_{i,1}
\end{aligned} \tag{2.74}$$

(2.73) and (2.74) constitute 2 equations per node. The number of unknowns per node is 4. The outgoing partial currents ($j_{i+1/2}^+, j_{i-1/2}^-$), the node flux ϕ_i , and the first moment of neutron flux $\phi_{i,1}$ constitute the four unknowns. The incoming partial currents ($j_{i-1/2}^+, j_{i+1/2}^-$) can be considered known quantities, since they are either equal to the outgoing partial currents of the neighboring nodes or are known from boundary condition.

The remarks above are valid if conventional homogenization theory is used and, thus continuity of partial currents is assumed. If equivalence homogenization theory is used; the incoming partial currents are not equal to the outgoing partial currents of the neighboring nodes. The incoming partial current can be written in terms of the outgoing partial current of the neighboring node, outgoing partial current of the same node and the flux discontinuity factors.

2.4 Nodal Balance Equation

The nodal view of the first order system (2.5) and (2.6) suggests that a natural starting point is to integrate the exact balance equation (2.5) over an arbitrary node

$$\int_{V_i} \nabla \cdot \mathbf{J}(\mathbf{r}) dV + \int_{\Sigma_r} \Sigma_r(\mathbf{r}) \phi(\mathbf{r}) dV = \int_{V_i} Q(\mathbf{r}) dV \tag{2.75}$$

In cylindrical coordinates, over radial component

$$2\pi \int_{r_{i-1/2}}^{r_{i+1/2}} \frac{1}{r} \frac{d}{dr} [rJ(r)] r dr + 2\pi \Sigma_r^i \int_{r_{i-1/2}}^{r_{i+1/2}} \phi(r) r dr = 2\pi \int_{r_{i-1/2}}^{r_{i+1/2}} Q(r) r dr \tag{2.76}$$

Since the node is already homogenized, macroscopic removal cross section is constant for a node, $\Sigma_r(r) = \Sigma_r^i$ and it is also assumed constant for all nodes of the same material, $\Sigma_r^i = \Sigma_r$. When the integrations are carried out with the help of (2.8) and (2.9), (2.17) becomes:

$$2\pi[r_{i+1/2}J_{i+1/2} - r_{i-1/2}J_{i-1/2}] + \frac{\Sigma_r\phi_i 2\pi(r_{i+1/2}^2 - r_{i-1/2}^2)}{2} = \frac{Q_i 2\pi(r_{i+1/2}^2 - r_{i-1/2}^2)}{2} \quad (2.77)$$

where ϕ_i and Q_i represent the node averaged flux and source respectively.

Surface areas can be defined as

$$S_{i+1/2} = 2\pi r_{i+1/2}, \text{ and } S_{i-1/2} = 2\pi r_{i-1/2} \quad (2.78)$$

Combining (2.7) and (2.19) with (2.18) gives

$$S_{i+1/2}J_{i+1/2} - S_{i-1/2}J_{i-1/2} + \frac{\Sigma_r\phi_i\Delta_i}{2}(S_{i+1/2} + S_{i-1/2}) = \frac{Q_i\Delta_i}{2}(S_{i+1/2} + S_{i-1/2}) \quad (2.79)$$

Surface areas at nodes are

$$S_i = 2\pi r_i \quad (2.80)$$

where r_i can be written as

$$r_i = \frac{r_{i+1/2} + r_{i-1/2}}{2} \quad (2.81)$$

Using (2.78) and (2.80)

$$S_i = \frac{S_{i+1/2} + S_{i-1/2}}{2} \quad (2.82)$$

Substituting (2.13), (2.14) and (2.81) into (2.78), finally, the discrete nodal balance equation

$$S_{i+1/2}(j_{i+1/2}^+ - j_{i+1/2}^-) - S_{i-1/2}(j_{i-1/2}^+ - j_{i-1/2}^-) + \Sigma_r\phi_i\Delta_i S_i = Q_i\Delta_i S_i \quad (2.83)$$

2.5 Weighted Residual Process - First Moment of Diffusion Equation

It was claimed that equations from Fick's law and nodal balance equation are not sufficient to solve the system for high order expansions. Therefore, moments are useful definitions, which help us in order to build a system. An n^{th} order expansion

needs to have n-2 moment(s), and weighted residual method should be applied n-2 times as well.

For the Cubic Expansion, first moment of diffusion equation is enough, and weighted residual process can be accomplished by the application of followings steps:

First of all, multiply both sides of diffusion equation by the first order polynomial,

$$\int_{V_i} w_1 \nabla \cdot J(r) dV + \int_{V_i} w_1 \sum_r \phi(r) dV = \int_{V_i} w_1 Q(r) dV \quad (2.84)$$

At this point, a return from normalized variable to real variable can be useful,

$$\xi = \frac{r - r_i}{\Delta_i}, \quad w_1(\xi) = P_1(\xi) = \xi \quad \Rightarrow \quad w_1(r) = \frac{r - r_i}{\Delta_i} \quad (2.85)$$

Divide the equation into 3 parts,

$$\underbrace{2\pi \int_{r_{i-1/2}}^{r_{i+1/2}} \frac{1}{r} \frac{d}{dr} [rJ(r)] P_1 r dr}_1 + \underbrace{2\pi \sum_r \int_{r_{i-1/2}}^{r_{i+1/2}} P_1 \phi(r) r dr}_2 = \underbrace{2\pi \int_{r_{i-1/2}}^{r_{i+1/2}} P_1 Q(r) r dr}_3 \quad (2.86)$$

For the first part, the integration in radial coordinates,

$$(1) = 2\pi \int_{r_{i-1/2}}^{r_{i+1/2}} \frac{1}{r} \frac{d}{dr} [rJ(r)] P_1 r dr \quad \Rightarrow \quad (1) = 2\pi \int_{r_{i-1/2}}^{r_{i+1/2}} \frac{1}{r} \frac{d}{dr} [rJ(r)] \left(\frac{r - r_i}{\Delta_i} \right) dr \quad (2.87)$$

Use Fick's law,

$$rJ(r) = -D_i r \frac{d\phi}{dr} \quad \Rightarrow \quad (1) = -2\pi D_i \int_{r_{i-1/2}}^{r_{i+1/2}} \frac{d}{dr} \left[r \frac{d\phi}{dr} \right] \left(\frac{r - r_i}{\Delta_i} \right) dr \quad (2.88)$$

Now, apply integration by parts,

$$\frac{d}{dr} \left[r \frac{d\phi}{dr} \right] dr = dv \quad \Rightarrow \quad v = r \frac{d\phi}{dr}, \quad u = \frac{r - r_i}{\Delta_i} \quad \Rightarrow \quad du = \frac{dr_i}{\Delta_i} \quad (2.89)$$

One can obtain

$$(1) = -2\pi D_i \left[\left(r \frac{d\phi}{dr} \right) \left(\frac{r - r_i}{\Delta_i} \right) \right]_{r_{i-1/2}}^{r_{i+1/2}} + 2\pi \frac{D_i}{\Delta_i} \int_{r_{i-1/2}}^{r_{i+1/2}} r \frac{d\phi}{dr} dr \quad (2.90)$$

Apply integration by parts for the term $2\pi \frac{D_i}{\Delta_i} \int_{r_{i-1/2}}^{r_{i+1/2}} r \frac{d\phi}{dr} dr$,

$$\frac{d\phi}{dr} dr = dv \Rightarrow v = \phi, \quad u = r \Rightarrow du = dr \quad (2.91)$$

After the definition of new variables, integral becomes

$$2\pi \frac{D_i}{\Delta_i} \int_{r_{i-1/2}}^{r_{i+1/2}} r \frac{d\phi}{dr} dr = 2\pi \frac{D_i}{\Delta_i} [r\phi]_{r_{i-1/2}}^{r_{i+1/2}} - 2\pi \frac{D_i}{\Delta_i} \int_{r_{i-1/2}}^{r_{i+1/2}} \phi dr \quad (2.92)$$

Hence, the first part

$$(1) = \underbrace{-2\pi D_i \left[\left(r \frac{d\phi}{dr} \right) \left(\frac{r-r_i}{\Delta_i} \right) \right]_{r_{i-1/2}}^{r_{i+1/2}}}_A + \underbrace{2\pi \frac{D_i}{\Delta_i} [r\phi]_{r_{i-1/2}}^{r_{i+1/2}}}_B - \underbrace{2\pi \frac{D_i}{\Delta_i} \int_{r_{i-1/2}}^{r_{i+1/2}} \phi dr}_C \quad (2.93)$$

the calculation of A, B, and C

$$(A) = -2\pi D_i \left[\left(r \frac{d\phi}{dr} \right) \left(\frac{r-r_i}{\Delta_i} \right) \right]_{r_{i-1/2}}^{r_{i+1/2}} = \frac{S_{i+1/2}}{2} \left(J_{i+1/2}^+ - J_{i+1/2}^- \right) - \frac{S_{i-1/2}}{2} \left(J_{i-1/2}^+ - J_{i-1/2}^- \right) \quad (2.94)$$

$$(B) = 2\pi \frac{D_i}{\Delta_i} [r\phi]_{r_{i-1/2}}^{r_{i+1/2}} = \frac{2D_i S_{i+1/2}}{\Delta_i} \left(J_{i+1/2}^+ - J_{i+1/2}^- \right) - \frac{2D_i S_{i-1/2}}{\Delta_i} \left(J_{i-1/2}^+ - J_{i-1/2}^- \right) \quad (2.95)$$

$$(C) = -2\pi \frac{D_i}{\Delta_i} \int_{r_{i-1/2}}^{r_{i+1/2}} \phi dr = -2\pi D_i a_0 \quad (2.96)$$

Now, the second part can be derived using the definitions. Recall that the first moment of neutron flux is

$$\phi_{i,1} = \frac{1}{\Delta_i r_i} \int_{-1/2}^{1/2} P_i(\xi) \phi(\xi) (\xi \Delta_i + r_i) \Delta_i d\xi = \frac{1}{\Delta_i r_i} \int_{r_{i-1/2}}^{r_{i+1/2}} P_i \phi(r) r dr \quad (2.97)$$

$$\begin{aligned}
(2) &= 2\pi \sum_r \int_{r_{i-1/2}}^{r_{i+1/2}} P_1 \phi(r) r dr = 2\pi \sum_r \left[\frac{\Delta_i r_i}{\Delta_i r_i} \int_{r_{i-1/2}}^{r_{i+1/2}} P_1 \phi(r) r dr \right] \\
&= 2\pi \sum_r \Delta_i r_i \underbrace{\left[\frac{1}{\Delta_i r_i} \int_{r_{i-1/2}}^{r_{i+1/2}} P_1 \phi(r) r dr \right]}_{\phi_{i,1}}
\end{aligned} \tag{2.98}$$

$$(2) = 2\pi \sum_r \Delta_i r_i \phi_{i,1} = S_i \sum_r \Delta_i \phi_{i,1} \tag{2.99}$$

The third part can be determined similarly,

$$(3) = 2\pi \int_{r_{i-1/2}}^{r_{i+1/2}} P_1 Q(r) r dr = 2\pi \int_{r_{i-1/2}}^{r_{i+1/2}} \frac{v \sum_f}{k} P_1 \phi(r) r dr \tag{2.100}$$

$$\begin{aligned}
(3) &= 2\pi \frac{v \sum_f}{k} \int_{r_{i-1/2}}^{r_{i+1/2}} P_1 \phi(r) r dr = 2\pi \frac{v \sum_f}{k} \left[\frac{\Delta_i r_i}{\Delta_i r_i} \int_{r_{i-1/2}}^{r_{i+1/2}} P_1 \phi(r) r dr \right] \\
&= 2\pi \frac{v \sum_f}{k} \Delta_i r_i \underbrace{\left[\frac{1}{\Delta_i r_i} \int_{r_{i-1/2}}^{r_{i+1/2}} P_1 \phi(r) r dr \right]}_{\phi_{i,1}}
\end{aligned} \tag{2.101}$$

$$(3) = 2\pi \frac{v \sum_f}{k} \Delta_i r_i \phi_{i,1} = \frac{v \sum_f S_i \Delta_i \phi_{i,1}}{k} \tag{2.102}$$

Finally, after simplifications and factorizations, the first moment of neutron diffusion equation

$$\begin{aligned}
&\left(\frac{4\pi D_i \alpha_i}{15} - \frac{S_{i-1/2}}{2} - \frac{2D_i S_{i-1/2}}{\Delta_i} \right) j_{i-1/2}^- + \left(\frac{4\pi D_i \alpha_i}{15} + \frac{S_{i-1/2}}{2} - \frac{2D_i S_{i-1/2}}{\Delta_i} \right) j_{i-1/2}^+ \\
&+ \left(\frac{4\pi D_i \alpha_i}{15} - \frac{S_{i+1/2}}{2} + \frac{2D_i S_{i+1/2}}{\Delta_i} \right) j_{i+1/2}^- + \left(\frac{4\pi D_i \alpha_i}{15} + \frac{S_{i+1/2}}{2} + \frac{2D_i S_{i+1/2}}{\Delta_i} \right) j_{i+1/2}^+ \\
&+ \left[8\pi D_i \alpha_i \left(\frac{r_i}{\Delta_i} \right)^2 \right] \phi_i + \left[S_i \sum_r \Delta_i - 8\pi D_i \alpha_i \left(\frac{r_i}{\Delta_i} \right) \right] \phi_{i,1} = \frac{v \sum_f S_i \Delta_i \phi_{i,1}}{k}
\end{aligned} \tag{2.103}$$

2.6 Formation of Iteration Matrix

2.6.1 Discretized Terms Revisited

$$\begin{aligned}
 (*) \quad j_{i+\frac{1}{2}}^+ &= \underbrace{\left(\frac{k_i + l_i y_i}{1 - l_i y_i} \right)}_{(C_1)_i} j_{i+\frac{1}{2}}^- + \underbrace{\left(\frac{l_i + l_i x_i}{1 - l_i y_i} \right)}_{(C_2)_i} j_{i-\frac{1}{2}}^- \\
 &+ \underbrace{\left[\frac{12 \left[2(m_i - l_i z_i) \left(\frac{r_i}{\Delta_i} \right)^2 + (-l_i z_i - m_i) \left(\frac{r_i}{\Delta_i} \right) \right]}{(1 - l_i y_i)} \right]}_{(C_3)_i} \phi_i \\
 &+ \underbrace{\left[\frac{24 \left[10(m_i + l_i z_i) \left(\frac{r_i}{\Delta_i} \right)^2 + (l_i z_i - m_i) \left(\frac{r_i}{\Delta_i} \right) \right]}{(1 - l_i y_i)} \right]}_{(C_4)_i} \phi_{i,1}
 \end{aligned} \tag{2.104}$$

$$\begin{aligned}
 (**) \quad &\underbrace{\left(\frac{4\pi D_i \alpha_i}{15} - \frac{S_{i-1/2}}{2} - \frac{2D_i S_{i-1/2}}{\Delta_i} \right)}_{(C_5)_i} j_{i-1/2}^- + \underbrace{\left(\frac{4\pi D_i \alpha_i}{15} + \frac{S_{i-1/2}}{2} - \frac{2D_i S_{i-1/2}}{\Delta_i} \right)}_{(C_6)_i} j_{i-1/2}^+ \\
 &+ \underbrace{\left(\frac{4\pi D_i \alpha_i}{15} - \frac{S_{i+1/2}}{2} + \frac{2D_i S_{i+1/2}}{\Delta_i} \right)}_{(C_7)_i} j_{i+1/2}^- + \underbrace{\left(\frac{4\pi D_i \alpha_i}{15} + \frac{S_{i+1/2}}{2} + \frac{2D_i S_{i+1/2}}{\Delta_i} \right)}_{(C_8)_i} j_{i+1/2}^+ \\
 &+ \underbrace{\left[8\pi D_i \alpha_i \left(\frac{r_i}{\Delta_i} \right)^2 \right]}_{(C_9)_i} \phi_i + \underbrace{\left[S_i \sum_r \Delta_i - 8\pi D_i \alpha_i \left(\frac{r_i}{\Delta_i} \right) \right]}_{(C_{10})_i} \phi_{i,1} = \frac{v \sum_r S_i \Delta_i \phi_{i,1}}{k}
 \end{aligned} \tag{2.105}$$

$$\begin{aligned}
 (***) \quad j_{i-\frac{1}{2}}^- &= \underbrace{\left(\frac{x_i + l_i y_i}{1 - l_i y_i} \right)}_{(C_{11})_i} j_{i-\frac{1}{2}}^+ + \underbrace{\left(\frac{y_i + y_i k_i}{1 - l_i y_i} \right)}_{(C_{12})_i} j_{i+\frac{1}{2}}^- \\
 &+ \underbrace{\left[\frac{12 \left[2(y_i m_i - z_i) \left(\frac{r_i}{\Delta_i} \right)^2 + (-z_i - y_i m_i) \left(\frac{r_i}{\Delta_i} \right) \right]}{(1 - l_i y_i)} \right]}_{(C_{13})_i} \phi_i \\
 &+ \underbrace{\left[\frac{24 \left[10(y_i m_i + z_i) \left(\frac{r_i}{\Delta_i} \right)^2 + (z_i - m_i y_i) \left(\frac{r_i}{\Delta_i} \right) \right]}{(1 - l_i y_i)} \right]}_{(C_{14})_i} \phi_{i,1}
 \end{aligned} \tag{2.106}$$

$$\underline{\underline{F}}_{\underline{\underline{N}}}^{4N \times 4N} = \begin{bmatrix} \underline{\underline{F}}_1^{(4 \times 4)} & \underline{\underline{0}}^{(4 \times 4)} & \dots & \underline{\underline{0}}^{(4 \times 4)} \\ \underline{\underline{0}}^{(4 \times 4)} & \underline{\underline{F}}_2^{(4 \times 4)} & \dots & \underline{\underline{0}}^{(4 \times 4)} \\ \vdots & \vdots & \ddots & \vdots \\ \underline{\underline{0}}^{(4 \times 4)} & \underline{\underline{0}}^{(4 \times 4)} & \dots & \underline{\underline{F}}_N^{(4 \times 4)} \end{bmatrix}_{4N \times 4N} \quad (2.116)$$

where F is a node-variant term, and its primal state

$$\underline{\underline{F}}_1^{(4 \times 4)} = \begin{bmatrix} 0 & 0 & 0 & 0 \\ 0 & (v \sum_f S_1 \Delta_1) & 0 & 0 \\ 0 & 0 & (v \sum_f S_1 \Delta_1) & 0 \\ 0 & 0 & 0 & 0 \end{bmatrix} \quad (2.117)$$

2.7 Group Dependency

The multigroup diffusion equations can be written as

$$\begin{aligned} -\vec{\nabla} \cdot D_1 \vec{\nabla} \phi_1 + \Sigma_{R1} \phi_1 &= \frac{1}{k_{\text{eff}}} \chi_1 Q \\ -\vec{\nabla} \cdot D_2 \vec{\nabla} \phi_2 + \Sigma_{R2} \phi_2 &= \frac{1}{k_{\text{eff}}} \chi_2 Q + \Sigma_{S1 \rightarrow 2} \phi_1 \\ &\vdots \\ -\vec{\nabla} \cdot D_G \vec{\nabla} \phi_G + \Sigma_{RG} \phi_G &= \frac{1}{k_{\text{eff}}} \chi_G Q + \Sigma_{S1 \rightarrow G} \phi_1 + \dots + \Sigma_{S(G-1) \rightarrow G} \phi_{G-1} \end{aligned} \quad (2.118)$$

It is assumed that there is no upscattering and fission source is defined as

$$Q(\mathbf{r}) = \sum_{g'=1}^G v_{g'} \Sigma_{fg'} \phi_{g'}(\mathbf{r}) \quad (2.119)$$

The spatial dependence of the fission source is identical in each group diffusion equation.

The multigroup weighted residuals becomes

$$\begin{aligned} -D_G 2\pi \int_{r_{i-1/2}}^{r_{i+1/2}} \nabla^2 \phi_G P_1 r dr + \Sigma_{RG} 2\pi \int_{r_{i-1/2}}^{r_{i+1/2}} \phi_G P_1 r dr &= 2\pi \int_{r_{i-1/2}}^{r_{i+1/2}} \frac{1}{k_{\text{eff}}} \chi_G Q P_1 r dr \\ + 2\pi \int_{r_{i-1/2}}^{r_{i+1/2}} (\Sigma_{S1 \rightarrow G} \phi_1 + \dots + \Sigma_{S(G-1) \rightarrow G} \phi_{G-1}) P_1 r dr & \end{aligned} \quad (2.120)$$

The multigroup system is solved by the Fission Source Power Iteration [9], and the eigenvalue of the system is obtained as the effective neutron multiplication factor. This eigenvalue is the positive, real and dominant eigenvalue which corresponds to non-negative neutron fluxes. Furthermore, CNEMR is using linear system solver subroutines [14] in order to find $\underline{\underline{J}}_N$ which contains the unknowns.

3 NUMERICAL APPLICATIONS

The formulations derived in the previous chapter have been implemented in the CNEMR code which is a computer program written in FORTRAN 90. This code and the numerical results obtained will be described in this chapter. Also comparison with FEM is made by using the results of a computer program, QFEMR. For analytical solutions, the reader is referred to the thesis by M. Mercimek [13].

3.1 One-group, Bare, Homogeneous Reactor

In this problem, a bare, cylindrical reactor of diameter 7.5cm is considered (Figure 3.1). Zero incoming current boundary condition ($j^- = 0$) is assumed at the surface of this cylinder. Effective multiplication factor of this system is determined using the one group cross sections $D=0.65\text{cm}$, $\Sigma_a=0.12\text{cm}^{-1}$ and $\nu\Sigma_f=0.185\text{cm}^{-1}$.

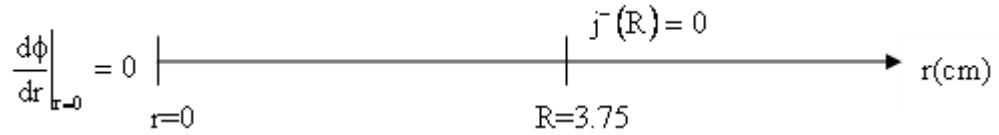


Figure 3.1 One-dimensional, Bare, Homogeneous, Cylindrical Reactor

3.1.1 Analytical Solution

One-group diffusion equation can be written as

$$\frac{1}{r} \frac{d}{dr} r \frac{d\phi(r)}{dr} - \frac{\Sigma_a \phi(r)}{D} = -\frac{1}{k_{\text{eff}}} \frac{\nu\Sigma_f}{D} \phi(r) \quad (3.1)$$

Simplifying (3.1)

$$\frac{1}{r} \frac{d}{dr} r \frac{d\phi(r)}{dr} + B^2 \phi(r) = 0 \quad (3.2)$$

where B is defined as

$$B^2 = \frac{\nu\Sigma_f - \Sigma_a}{D} \quad (3.3)$$

Solution of (3.2) is

$$\phi(r) = AJ_0(Br) \quad (3.4)$$

Zero incoming current boundary condition is

$$j^-(R) = \frac{\phi(R)}{4} + \frac{D}{2} \frac{d\phi}{dr} \Big|_{r=R} = 0 \quad (3.5)$$

Using (3.4) in (3.5) gives

$$J_0(BR) = 2DBJ_1(BR) \quad (3.6)$$

(3.6) can be written as

$$J_0(x) = \frac{2Dx}{R} J_1(x) \quad (3.7)$$

where $x=BR$. Substituting the numerical values of D and R in (3.7) gives

$$2.884615382J_0(x) - xJ_1(x) = 0 \quad (3.8)$$

(3.8) can be solved by using Newton's Method [15]

$$x^{(t+1)} = x^{(t)} - \frac{f(x^{(t)})}{f'(x^{(t)})} \quad (3.9)$$

where, t is the iteration number. Here $f(x)$ is the left hand side of (3.8). $f'(x)$ can be found using recurrence relation for Bessel Function of first kind,

$$xJ_n' = nJ_n - xJ_{n+1} = -nJ_n + xJ_{n-1} \quad (3.10)$$

Thus, (3.9) becomes

$$x^{(t+1)} = x^{(t)} + \frac{2.884615382J_0(x^{(t)}) - x^{(t)}J_1(x^{(t)})}{2.884615382J_1(x^{(t)}) + x^{(t)}J_0(x^{(t)})} \quad (3.11)$$

Initial estimate of $x^{(0)}$ can be found by assuming critical reactor, $k_{eff}=1$. In this case, (3.3) gives $B=0.316227766$ and $x^{(0)}=BR=1.185854123$. Table 3.1 shows the results of Newton's method.

Table 3.1 Iteration Steps of Newton's Method for the Solution of (3.7)

t	$x^{(t)}$	$\varepsilon^{(t)}$ (%)
0	1.185854123	-
1	1.799773445	94.9837
2	1.771173535	1.6145
3	1.771285989	0.0063
4	1.771285991	9.114×10^{-8}

These calculations are made using MATHEMATICA 5.2. Finally, $x=1.771285991$ and $B=x/R=0.47234293\text{cm}^{-1}$. Effective multiplication factor can be calculated as

$$k_{\text{eff}} = \frac{v\Sigma_f}{DB^2 + \Sigma_a} = 0.698060264 \quad (3.12)$$

Average flux is defined as

$$\bar{\phi} = \frac{\int_0^R \phi(r) 2\pi r dr}{\pi R^2} \quad (3.13)$$

Average flux can be calculated from (3.13)

$$\bar{\phi} = \frac{2}{R^2} \int_0^R A J_0(0.47234293r) r dr = 0.58086137546A \quad (3.14)$$

In order to find an expression for A, it is necessary to make a separate calculation of the reactor power. In particular, there are $\Sigma_f \phi(r)$ fissions per cm^3/sec at the point of r, and if the recoverable energy is w_f joules per fission ($w_f=3.2 \times 10^{-11}$ joules), then the total power per axial distance, in watts/cm, is

$$P = w_f \Sigma_f \int_0^R \phi(r) 2\pi r dr \quad (3.15)$$

Performing the integration gives

$$P = w_f \Sigma_f \pi R^2 0.58086137546A \quad (3.16)$$

If the reactor power is given as $P=2000\text{watt/cm}$, and the macroscopic fission cross section is $\Sigma_f=0.0764\text{cm}^{-1}$, then A is calculated as

$$A = \frac{P}{w_f \Sigma_f \pi R^2 0.58086137546} = 3.1894954 \times 10^{13} \quad (3.17)$$

Flux distribution can be found by multiplying constant A with cell average fluxes. Finally, average flux is calculated using (3.16) in (3.14) as

$$\bar{\phi} = 1.852654684 \times 10^{13} \text{ n}^0/\text{cm}^2\text{sec.} \quad (3.18)$$

3.1.2 Geometrical Discretization(2 nodes)

Here, formulations derived in previous section are tested with two node calculations before their implementation into the computer program. Figure 3.2 shows the nodes of this system. Since Δ and D are the same for the same material in one-group calculation, τ is the same for two nodes. From (2.73),

$$\tau = 12.3152$$

Δ is calculated by dividing radius, R by the number of nodes, 2. Therefore

$$\Delta = 1.875$$

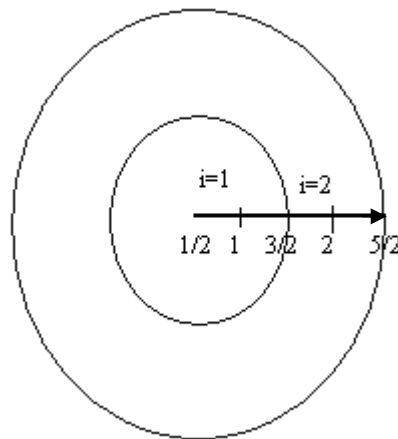


Figure 3.2 Cylindrical Reactor with Two Nodes

Radii and corresponding surface areas are given in Table 3.2. They are used in (2.76) through (2.80).

Table 3.2 Radii and Related Surface Areas

i	r_i (cm)	S_i (cm²)
1/2	0	0
1	0.9375	5.8875
3/2	1.8750	11.7750
2	2.8125	17.6625
5/2	3.7500	23.5500

3.1.3 CNEMR and QFEMR Results

Cubic NEM, Quadratic NEM, Linear FEM, and quadratic FEM results of effective neutron multiplication factor are given in Table 3.3

Table 3.3 k_{eff} Results of QFEMR and CNEMR Programs

Method	Number of Elements(FEM) or Nodes(NEM)	k_{eff}	Error (%)
Linear FEM	2	0.746411132	6.92646
	10	0.699714822	0.23702
	50	0.698125364	0.00933
	100	0.698076062	0.00226
Quadratic FEM	1	0.720881392	3.26922
	2	0.699073117	0.14509
	10	0.698061073	0.0001158
	50	0.698059636	0.00009
Quadratic NEM	3	0.694169485	0.55737
	5	0.696634106	0.204303
	11	0.697764156	0.042418
	21	0.697979689	0.011543
Cubic NEM	3	0.696976545	0.1552
	5	0.697824723	0.0332
	7	0.697985806	0.010668
	9	0.698037814	0.003217
	11	0.698060852	0.0000825
	13	0.698070554	0.001472
	15	0.698075272	0.002148
21	0.698078962	0.002677	

N elements correspond to N+1 node in the linear FEM. In case of quadratic finite elements, the number of nodes per element increases to three. N quadratic elements contain 2N+1 nodes.

Cubic NEM gets the best result for 3 nodes, which means it shows its coarse mesh behavior. Error percentage is decreasing while the node number is increasing. When the all node numbers are examined, Cubic NEM performance is obviously better than Quadratic NEM, and Linear NEM gets dramatically the worst results in all cases. If the node number is between 11 and 13, unexpected oscillation occurs in error percentages of Cubic NEM. In contrast, this situation doesn't exist in Quadratic

NEM. For the large numbers of node, Quadratic FEM reflects the most correct results thanks to its fine mesh property. The variation of k_{eff} obtained from 4 methods is shown in figure 3.3.

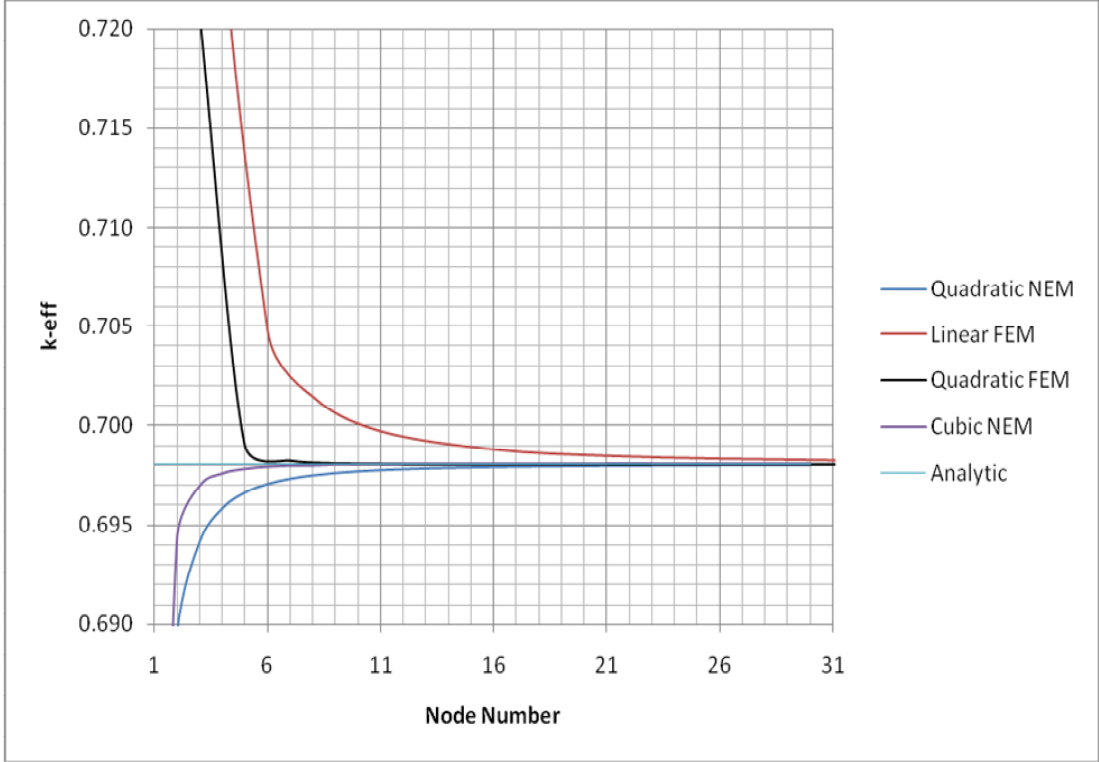


Figure 3.3 k_{eff} Results of FEM and NEM

Nodal Expansions from both degrees are converging from the values lower than analytical solution as it is shown in figure 3.3; however, FEM is converging from the values higher than analytical solution. Moreover, the rate of decrement is high between 3-6 nodes for the error values of Quadratic FEM. On the other hand, Linear FEM is approaching slowly to the analytical solution. The variation of error percentage of both Nodal Expansions is sketched in figure 3.4 to emphasize the advantage of cubic expansion.

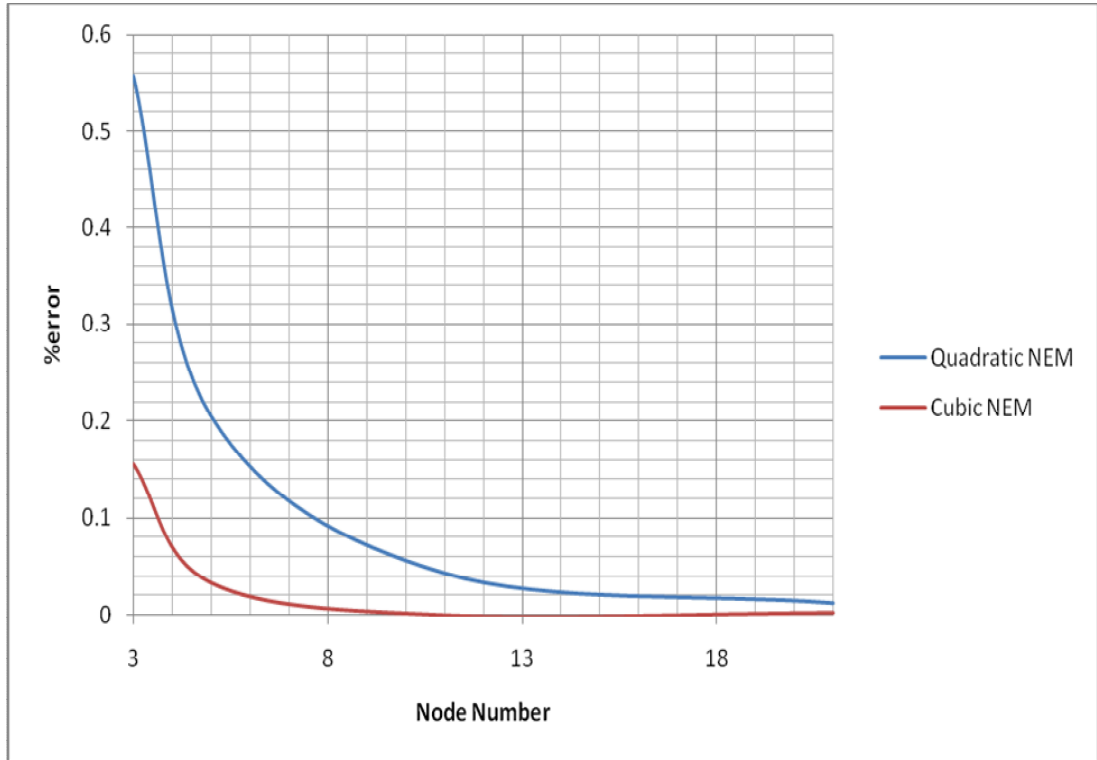


Figure 3.4 k_{eff} %error Variation

The error percentage variation of two expansions reveals that Cubic expansion results are better than Quadratic expansion results for all numbers of node. The ratio of error percentages is increasing slowly with respect to node number. For example, the ratio of Quadratic and Cubic NEM error percentage is 3.567 when the node number is 3. For 21 nodes, this ratio becomes 4.312. Furthermore, both error percentage functions behave like exponentially decreasing function.

In order to determine neutron flux, (3.13) can be discretized as

$$\bar{\phi} = \frac{\sum_{i=1}^N \phi_i S_i}{\sum_{i=1}^N S_i} \quad (3.19)$$

CNEMR calculates average flux using (3.19). They are given in table 3.4 with linear FEM results. Comparison with analytical result shows that CNEMR is able to calculate average flux with small error percentage. The values of NEM are so close; in addition, Linear NEM gets similar results as well. Moreover, the error values are sometimes increasing although node number is increasing. This effect is observed in three methods.

Table 3.4 Average Fluxes and Respective Errors

Method	Number of Nodes	$\bar{\phi} \times 10^{-13}$ (n ⁰ /cm ² sec.)	Error (%)
Quadratic NEM	3	1.851715510	0.050693418
	5	1.851715485	0.050694768
	11	1.851715342	0.050702486
	21	1.851715253	0.050707290
Cubic NEM	3	1.851715451	0.050696604
	5	1.851715260	0.050706913
	11	1.851715429	0.050697791
	21	1.851715147	0.050713012
Linear FEM	2	1.851715400	0.050699356
	10	1.851715400	0.050699356

CNEMR can calculate cell average fluxes with small error. Flux distributions are given in figure 3.5 for 31 nodes in both Nodal expansions.

It is shown in figure 3.5 that both Cubic and Quadratic NEM graphs are superimposed. Maximum flux is approximately 2.83×10^{13} n⁰/cm²sec at the center of the cylinder when the reactor power is taken to be 2000 W/cm.

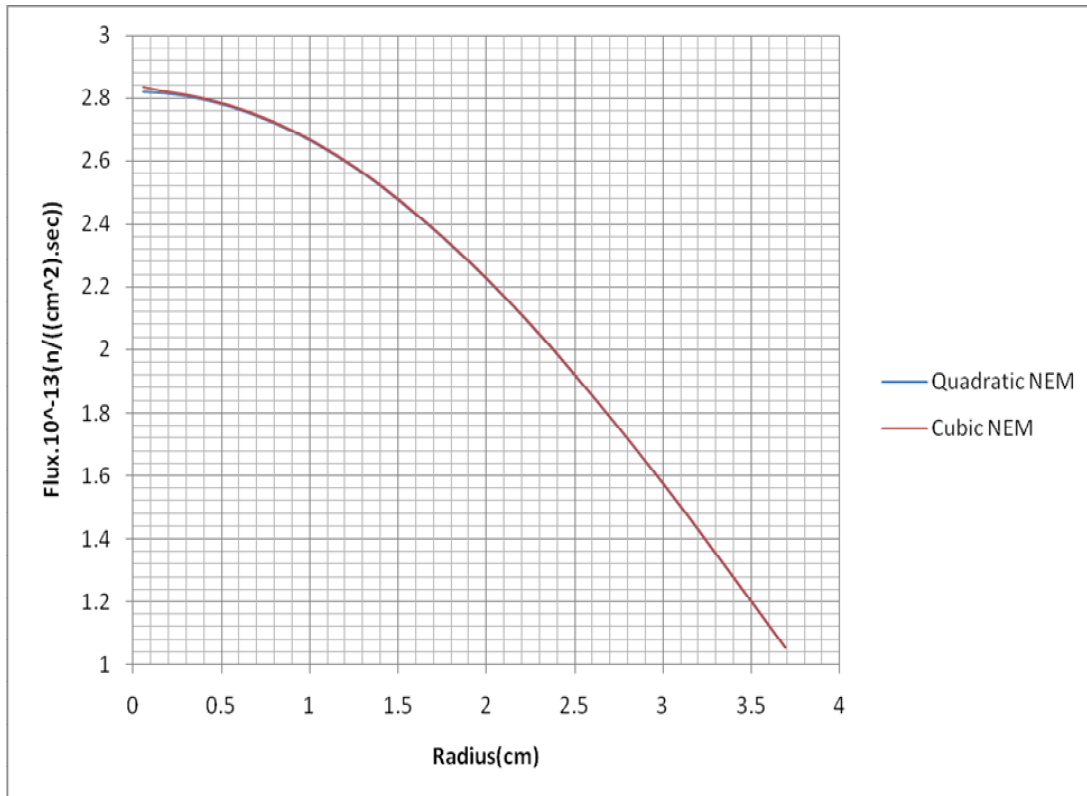


Figure 3.5 Flux Distribution Along the Radial Distance

3.2 One-Group Reflected Reactor

In this section, two-region cylindrical reactor is considered. It is composed of a central cylinder of one fuel-bearing material (region 1) embedded in an annulus of a second reflector material (region 2). It is assumed that multigroup spectra have been determined for the different (nuclearly homogeneous) materials in regions (1) and (2) and that the one-group cross-sections have been obtained by averaging over these spectra.

Fuel-bearing material is the same with the material defined in section 3.1. It has the same cross-sections and the same radius, $R_1=3.75\text{cm}$.

Reflector is a graphite material with thickness 1.25cm. Hence $R_2=5\text{cm}$. Absorption cross-section and diffusion coefficient of the graphite are taken to be 0.00032cm^{-1} and 0.84cm respectively.

3.2.1 Analytical Solution

The resulting form of the one-group diffusion equation is thus

$$D^k \left(\frac{1}{r} \frac{d}{dr} r \frac{d}{dr} \phi(r) \right) + \left(\frac{1}{\lambda} \nu \Sigma_f^k - \Sigma_a^k \right) \phi(r) = 0 \quad (3.20)$$

Continuity and boundary conditions are

$$\phi(R_1)^- = \phi(R_1)^+ \quad (3.21)$$

$$D^{(1)} \frac{d\phi(R_1)}{dr} \Big|^- = D^{(2)} \frac{d\phi(R_1)}{dr} \Big|^+ \quad (3.22)$$

$$\frac{1}{4} \phi(R_2) + \frac{D^{(2)}}{2} \frac{d}{dr} \phi(R_2) = 0 \quad (3.23)$$

where R_1 and R_2 are the radii of the fuel-bearing material and the reflector respectively. If one defines

$$(\kappa^k)^2 = \frac{\lambda^{-1} \nu \Sigma_f^k - \Sigma_a^k}{D^k} \quad (k = 1, 2) \quad (3.24)$$

(3.20) can be written as:

$$\left(\frac{1}{r} \frac{d}{dr} r \frac{d}{dr} \phi(r) \right) + (\kappa^k)^2 \phi(r) = 0 \quad (3.25)$$

Note that, (κ^k) can be real or pure imaginary depending on the magnitudes of the reactor parameters. It takes the form

$$(\kappa^F)^2 = \frac{\lambda^{-1} \nu \Sigma_f^F - \Sigma_a^F}{D^F} \quad (\text{Fuel region, real}) \quad (3.26)$$

$$(\kappa^R)^2 = \frac{\Sigma_a^R}{D^R} \quad (\text{Reflector region, imaginary}) \quad (3.27)$$

κ^F is real if $\lambda^{-1} \nu \Sigma_f^F \geq \Sigma_a^F$. Therefore, $\lambda \leq (\nu \Sigma_f^F / \Sigma_a^F = 1.54)$. Since the reflector can not increase the effective multiplication factor so much, the solution in the fuel region is

$$\phi_F(r) = C_1 J_0(\kappa^F r) \quad (3.28)$$

where J_0 is the zeroth-order Bessel function of the first kind. For the reflector region

$$\phi_R(r) = C_3 I_0(\kappa^R r) + C_4 K_0(\kappa^R r) \quad (3.29)$$

where I_0 and K_0 are zeroth-order modified Bessel functions of the first and second kind respectively. Applying zero incoming current boundary condition (3.23) to the (3.29) gives

$$C_3 = -C_4 \left[\frac{K_0(\kappa^R R_2) - 2D^R \kappa^R K_1(\kappa^R R_2)}{I_0(\kappa^R R_2) + 2D^R \kappa^R I_1(\kappa^R R_2)} \right] = -C_4 L \quad (3.30)$$

(3.29) becomes

$$\phi_R(r) = C_4 (-L I_0(\kappa^R r) + K_0(\kappa^R r)) \quad (3.31)$$

The continuity conditions at $r=R_1$, (3.21) and (3.22) now require that

$$C_1 J_0(\kappa^c R_1) = C_4 (-L I_0(\kappa^R R_1) + K_0(\kappa^R R_1)) \quad (3.32)$$

$$-C_1 D^c \kappa^c J_1(\kappa^c R_1) = C_4 D^R (-L \kappa^R I_1(\kappa^R R_1) - \kappa^R K_1(\kappa^R R_1)) \quad (3.33)$$

The critical equation may be obtained by dividing the first equation (3.32) into the second (3.33)

$$\frac{J_0(\kappa^c R_1)}{D^c \kappa^c J_1(\kappa^c R_1)} = \frac{-L I_0(\kappa^R R_1) + K_0(\kappa^R R_1)}{D^R (L \kappa^R I_1(\kappa^R R_1) + \kappa^R K_1(\kappa^R R_1))} \quad (3.34)$$

RHS of (3.34) is calculated using MATHEMATICA 5.2

$$\frac{J_0(\kappa^c R_1)}{D^c \kappa^c J_1(\kappa^c R_1)} = 2.7822129453 \quad (3.35)$$

(3.35) can be re-arranged as

$$J_0(\kappa^c R_1) - 1.8084384144 \kappa^c J_1(\kappa^c R_1) = 0 \quad (3.36)$$

(3.36) would be suitable for the Newton's Method, if it is written as

$$f(x) = J_0(x) - 0.482250243x J_1(x) = 0 \quad (3.37)$$

where $x = \kappa^c R_1$.

Newton's Method, (3.9), takes the form

$$x^{(t+1)} = x^{(t)} + \frac{J_0(x^{(t)}) - 0.482250243x^{(t)} J_1(x^{(t)})}{J_1(x^{(t)}) + 0.482250243x^{(t)} J_0(x^{(t)})} \quad (3.38)$$

Table 3.5 shows the steps of this iteration process, (3.38)

Table 3.5 Iteration Results of Newton Method

t	$x^{(t)}$	$\varepsilon^{(t)}(\%)$
0	1	40.599315
1	1.683482	4.13843
2	1.61658	0.0276963
3	1.61703	9.32603×10^{-7}
4	1.61702907	1.37316×10^{-14}

Thus

$$\kappa^c = \frac{x}{R_1} = 0.431207753 \quad (3.39)$$

Effective multiplication factor is found analytically from (3.39) as

$$\lambda = k_{\text{eff}} = 0.768077605 \quad (3.40)$$

From (3.13) and (3.15) average flux is

$$\bar{\phi} = \frac{P}{w_f \Sigma_f \pi R_1^2} \quad (3.41)$$

Average flux in the fuel region is the same as calculated in section (3.1.1) and given in (3.17). $\bar{\phi}_F = 1.852654684 \times 10^{13} \text{ n}^0/\text{cm}^2\text{sec}$, since all variables of (3.41) remains the same.

But, it is complicated to find the average flux in the reflector. First, it is necessary to find C_1 in (3.28)

$$\bar{\phi}_F = \frac{2}{R_1^2} \int_0^{R_1} C_1 J_0(0.431207753r) r dr \quad (3.42)$$

This integral is evaluated by using the following recursion formula

$$\int x^n J_{n-1}(x) dx = x^n J_n(x) \quad (3.43)$$

Thus

$$\bar{\phi}_F = 0.706884906 C_1 \quad (3.44)$$

From (3.17)

$$C_1 = 2.620871754 \times 10^{13} \quad (3.45)$$

Next, C_4 is found from (3.32)

$$C_4 = \frac{C_1 J_0(\kappa^R R_1)}{(-LI_0(\kappa^R R_1) + K_0(\kappa^R R_1))} = 1.87991806 \quad (3.46)$$

Average flux in the reflector is defined as

$$\bar{\phi}_R = \frac{\int_{R_1}^{R_2} \phi_R(r) 2\pi r dr}{\pi(R_2^2 - R_1^2)} \quad (3.47)$$

Substituting (3.31) into (3.47)

$$\bar{\phi}_R = \frac{2C_4}{(R_2^2 - R_1^2)} \left[- \int_{R_1}^{R_2} LI_0(\kappa^R r) r dr + \int_{R_1}^{R_2} K_0(\kappa^R r) r dr \right] \quad (3.48)$$

These integrals are evaluated using the following recursion formulas

$$\int x^n I_{n-1}(x) dx = x^n I_n(x) \quad \text{and} \quad \int x^n K_{n-1}(x) dx = -x^n K_n(x) \quad (3.49)$$

Final equation for the average flux in the reflector is

$$\bar{\phi}_R = \frac{-2C_4}{(R_2^2 - R_1^2)(\kappa^R)^2} (L\kappa^R R_2 I_1(\kappa^R R_2) - L\kappa^R R_1 I_1(\kappa^R R_1) + \kappa^R R_2 K_1(\kappa^R R_2) - \kappa^R R_1 K_1(\kappa^R R_1)) \quad (3.50)$$

Average flux has been calculated from (3.50) using MATHEMATICA 5.2

$$\bar{\phi}_R = 8.728700636172 \times 10^{12} \text{ n}^0/\text{cm}^2\text{sec.} \quad (3.51)$$

3.2.2 CNEMR and QFEMR Results

The effective neutron multiplication factors obtained by NEM and FEM are shown in Table 3.6 with their error percentages. As in the previous situation, NEM gives the best results for initial nodes.

Table 3.6 Effective Multiplication Factors Calculated by 4 Methods

Number of Nodes			k_{eff}	Error (%)
Quadratic NEM				
Fuel	Refl.	Total		
2	1	3	0.76390350	0.5434
3	2	5	0.76581560	0.2945
4	3	7	0.76673990	0.1742
6	3	9	0.76756920	0.0662
7	4	11	0.76767430	0.0525
Cubic NEM			k_{eff}	Error (%)
Fuel	Refl.	Total		
2	1	3	0.76284032	0.6819
3	2	5	0.76627059	0.2353
4	3	7	0.76720524	0.1136
6	3	9	0.76776720	0.0404
7	4	11	0.76787128	0.0269
Number of Elements and Total Nodes			k_{eff}	Error (%)
Linear FEM				
Fuel (El.)	Refl. (El.)	Total (Node)		
1	1	3	0.99030426	28.9328
2	2	5	0.80352910	4.6156
4	2	7	0.77568958	0.9910
5	3	9	0.77290074	0.6279
7	3	11	0.77046017	0.3102
Quadratic FEM			k_{eff}	Error (%)
Fuel	Refl.	Total		
1	1	5	0.78547520	2.2651
2	1	7	0.76887844	0.1043
2	2	9	0.76888222	0.1047
3	2	11	0.76822594	0.0193
4	2	13	0.76812242	0.0058

Especially, Quadratic NEM has the smallest error for 3 nodes; however, Cubic NEM gets better results for the other numbers of node. The increase of the nodes in the fuel region improves k_{eff} value more than the reflector, since the fuel region is a multiplier medium for neutrons, and the radius of the fuel is greater than the radius of the reflector.

When the number of nodes is 7, there exists small difference between error values of Quadratic FEM and Cubic NEM, but if it is 9, NEM seems better unexpectedly. It is claimed that number of nodes in the fuel region is larger than the reflector region in NEM. But, quadratic FEM puts the same number of elements, 2, into both regions although the total number of nodes is the same in both methods. Therefore, NEM gives more accurate result than quadratic FEM, for fuel region is generating the neutron multiplication. After 9 nodes, quadratic FEM gives better results than other methods. Linear NEM shows the worst results again.

One can conclude that NEM is more advantageous than linear and quadratic FEM due to its faster convergence using the coarse mesh. While the mesh is getting finer, number of nodes is increased and quadratic FEM becomes more advantageous than other methods. This is shown in figure 3.6.

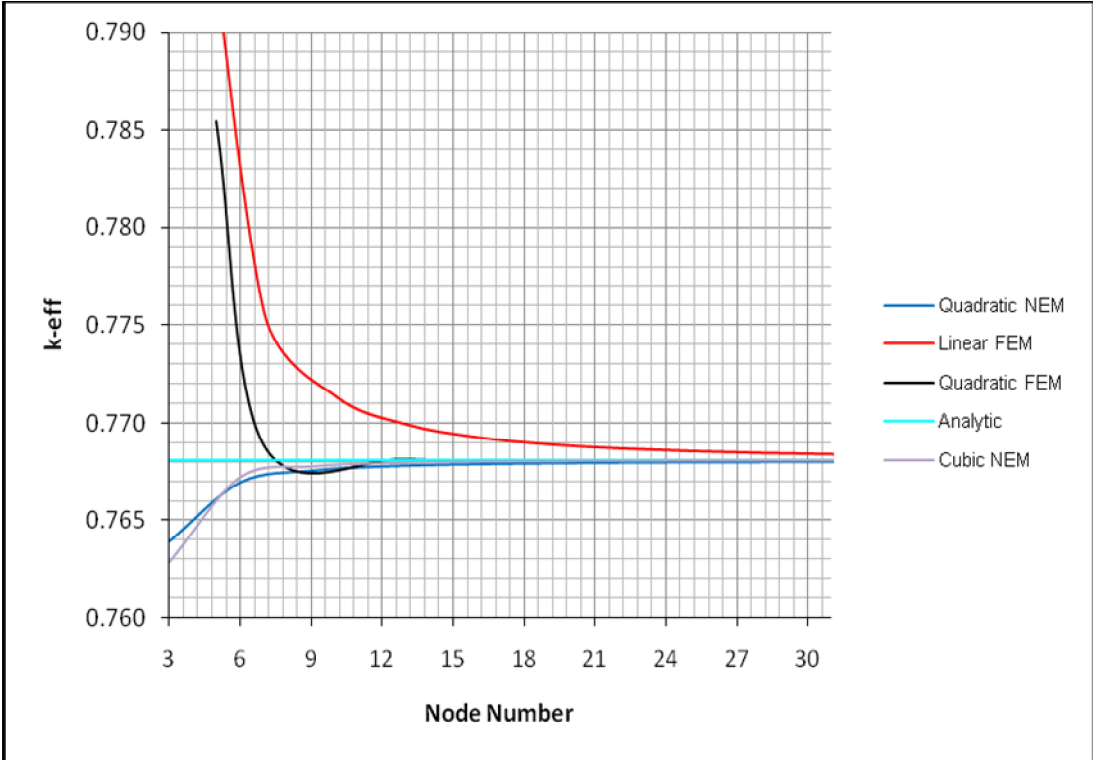


Figure 3.6 Variation of k_{eff} with Respect to Total Number of Nodes

Nodal Expansions from both degrees are converging from the values lower than analytical solution as it is shown in figure 3.6; on the other hand, Linear FEM is converging from the values higher than analytical solution. Quadratic FEM starts with the values higher than the analytical solutions, gets results lower than the reference solution when the corresponding node number is between 8 and 11.

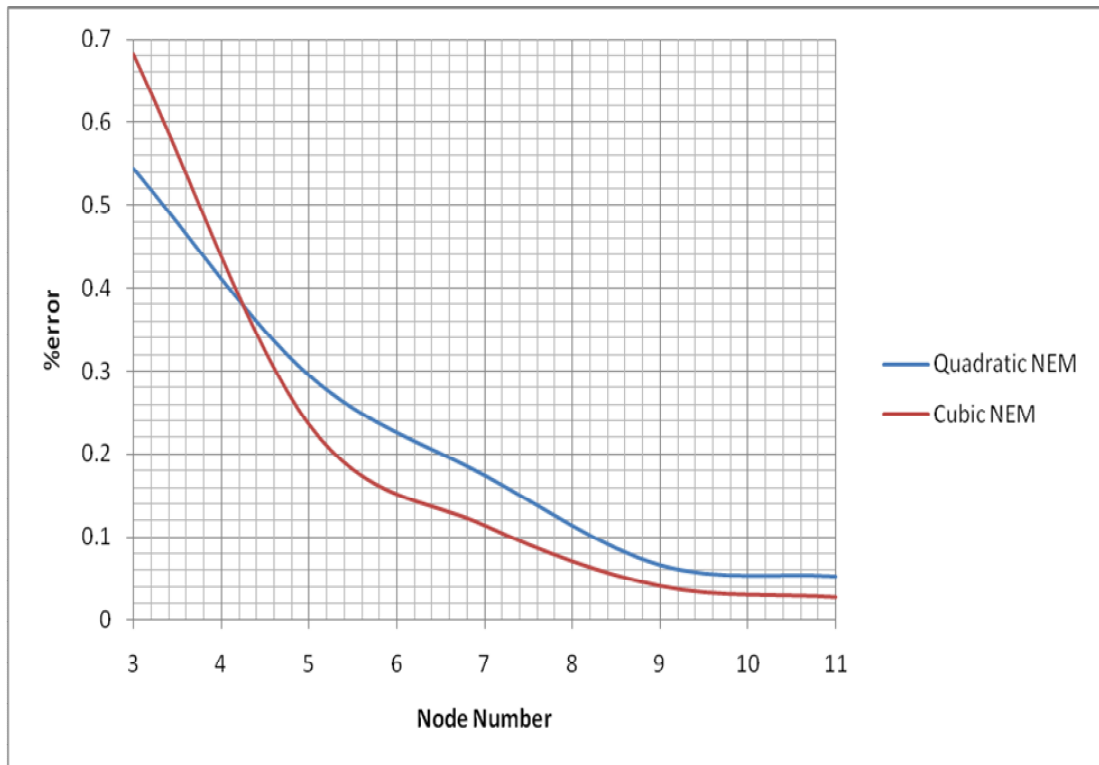


Figure 3.7 k_{eff} %error Variation

The comparison of NEM error percentages is illustrated in Figure 3.7. Cubic NEM has better results for all numbers of node except initial trials. After 4 nodes, the difference between errors is getting larger, and it becomes stable after 9 nodes.

Table 3.7 shows the average fluxes calculated in the fuel and the reflector regions. Both methods calculate average fluxes accurately in the fuel region with very small and similar error values. The ratio between the number of nodes or elements of the fuel and reflector is selected as 2. In the reflector, Cubic NEM is the fastest method which converges to the analytical solution. For example, Cubic NEM gets 2.5 times better result than Quadratic NEM although the node number is 9 for Cubic and 10 for Quadratic. A surprising point is that the error percentages of Cubic NEM are increasing between 9 and 30 nodes despite of the node augmentation. Similar effect is observed in the error values of Quadratic NEM between 20 and 30 nodes.

Table 3.7 Average Fluxes with Their Errors in The Fuel and The Reflector

	Number of Nodes			$\bar{\phi}_F \times 10^{-13}$	Error (%) (Fuel)	$\bar{\phi}_R \times 10^{-13}$	Error (%) (Reflector)
	Fuel	Reflector	Total				
Quadratic NEM	3	2	5	1.851715477	0.050695200	0.878367521	0.629813968
	7	3	10	1.851715418	0.050698385	0.873525390	0.075077163
	14	6	20	1.851715457	0.050696280	0.872703571	0.019074193
	20	10	30	1.851715756	0.050680141	0.872564972	0.034952673
Cubic NEM	4	2	6	1.851715421	0.050698223	0.874402950	0.175614464
	6	3	9	1.851715455	0.050696388	0.873133308	0.030158507
	12	6	18	1.851715457	0.050696280	0.872519172	0.04019972
	20	10	30	1.851715302	0.050704646	0.872424767	0.05101519
	Number of Elements						
Linear FEM	Fuel	Reflector	Total				
	2	2	4	1.851715400	0.050699336	0.798289649	8.544274488
	6	3	9	1.851715400	0.050699336	0.866251779	0.758221061
	13	6	19	1.851715400	0.050699336	0.871193009	0.192131084
	19	10	29	1.851715400	0.050699336	0.871814416	0.120939875

In figure 3.8, flux distribution along the radius of the cylinder are shown for 30 nodes, 20 fuel and 10 reflector. It is appeared that two graphs overlap. Hence, two expansions find approximately the same fluxes.

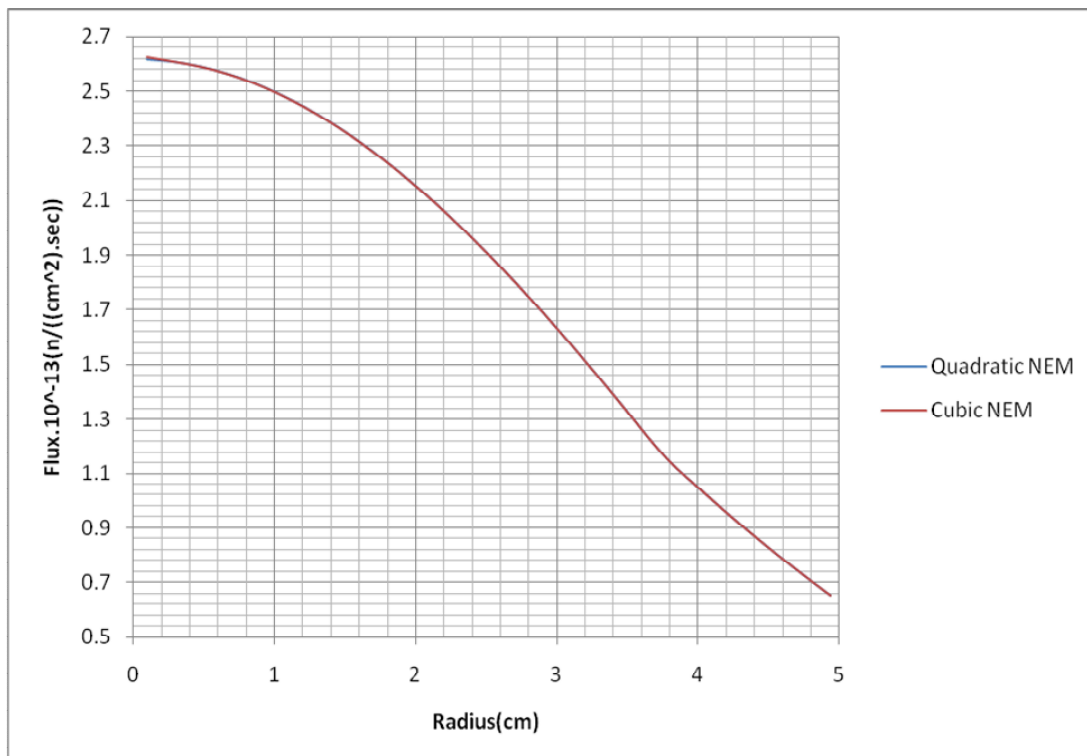


Figure 3.8 Flux Distribution in the Reflected Reactor

3.3 Two-group, Bare, Homogeneous Reactor

In this problem, two-group analysis of a bare, cylindrical reactor is developed. First, critical radius is calculated for zero incoming current boundary condition. Then, QFEMR and CNEMR results are compared to see how close they can calculate k_{eff} to critical value. Two-group parameters are given as

$$D_1=1.2627\text{cm}, \quad \Sigma_{R1}=0.02619\text{cm}^{-1}, \quad \Sigma_{S,1\rightarrow 2}=0.01412\text{cm}^{-1}, \quad \nu_1\Sigma_{f,1}=0.008476\text{cm}^{-1}, \\ D_2=0.3543\text{cm}, \Sigma_{a,2}=0.1210\text{cm}^{-1}, \nu_2\Sigma_{f,2}=0.18514\text{cm}^{-1} \text{ and } \chi_1=1, \chi_2=0.$$

Reactor power is taken to be 2000W/cm as in the previous problems.

3.3.1 Analytical Solution

Two-group diffusion equations can be written as

$$-\vec{\nabla} \cdot D_1 \vec{\nabla} \phi_1 + \Sigma_{R1} \phi_1 = \frac{1}{k_{\text{eff}}} [\nu_1 \Sigma_{f1} \phi_1 + \nu_2 \Sigma_{f2} \phi_2] \quad (3.52)$$

$$-\vec{\nabla} \cdot D_2 \vec{\nabla} \phi_2 + \Sigma_{a2} \phi_2 = \Sigma_{S,1\rightarrow 2} \phi_1 \quad (3.53)$$

Since the reactor is critical $k_{\text{eff}}=1$. Assuming, thermal to fast flux ratio is constant and defined by

$$S = \frac{\phi_2}{\phi_1} \quad (3.54)$$

using (3.54) in (3.52) and (3.53) gives respectively

$$\frac{1}{r} \frac{d}{dr} r \frac{d\phi_1}{dr} + \frac{(\nu_1 \Sigma_{f1} + \nu_2 \Sigma_{f2} S - \Sigma_{R1})}{D_1} \phi_1 = 0 \quad (3.55)$$

$$\frac{1}{r} \frac{d}{dr} r \frac{d\phi_2}{dr} + \frac{(\Sigma_{S,1\rightarrow 2}/S - \Sigma_{a2})}{D_2} \phi_2 = 0 \quad (3.56)$$

Fast and thermal group buckling terms are defined as

$$B_1^2 = \frac{(\nu_1 \Sigma_{f1} + \nu_2 \Sigma_{f2} S - \Sigma_{R1})}{D_1} \quad (3.57)$$

$$B_2^2 = \frac{(\Sigma_{S,1\rightarrow 2}/S - \Sigma_{a2})}{D_2} \quad (3.58)$$

Solutions of (3.55) and (3.56) are given by

$$\phi_1(r) = C_1 J_0(B_1 r) \quad (3.59)$$

$$\phi_2(r) = C_2 J_0(B_2 r) \quad (3.60)$$

Next, applying zero incoming current boundary condition, (3.5) to (3.59) and (3.60) yields

$$J_0(B_1 R) = 2B_1 D_1 J_1(B_1 R) \quad (3.61)$$

$$J_0(B_2 R) = 2B_2 D_2 J_1(B_2 R) \quad (3.62)$$

(3.61) and (3.62) are solved iteratively using Newton's Method, (3.9). Then

$$f(x) = J_0(x) - 2B_1 D_1 J_1(x) \quad (3.63)$$

$$f(y) = J_0(y) - 2B_2 D_2 J_1(y) \quad (3.64)$$

where $x=B_1 R$ and $y=B_2 R$. Applying Newton's Method to (3.63) and (3.64) gives

$$x^{(t+1)} = x^{(t)} - \frac{(J_0(x^{(t)}) - 2B_1 D_1 J_1(x^{(t)}))}{(J_1(x^{(t)})(2B_1 D_1 - 1) - 2B_1 D_1 J_0(x^{(t)}))} \quad (3.65)$$

$$y^{(t+1)} = y^{(t)} - \frac{(J_0(y^{(t)}) - 2B_2 D_2 J_1(y^{(t)}))}{(J_1(y^{(t)})(2B_2 D_2 - 1) - 2B_2 D_2 J_0(y^{(t)}))} \quad (3.66)$$

Before iteration, initial estimates of buckling terms are needed. From (3.58)

$$S = \frac{\Sigma_{S,1 \rightarrow 2}}{D_2 B_2^2 + \Sigma_{a2}} \quad (3.67)$$

First, initial value of B_2 is estimated. Next, this value is used in (3.65) and flux ratio, S is found. Then, S is used in (3.57) and new value of B_1 is found. B_1 and B_2 are used in (3.65) and (3.66). Also, initial x and y values are estimated with initial critical radius. Solution to this problem with zero flux condition at $r=R$ gives the geometric buckling and the critical radius as $B=0.05418\text{cm}^{-1}$, $R=44.3889\text{cm}$ [16]. So, initial B_2 and R values are taken to be 0.06cm^{-1} and 42.0cm respectively.

After the first iteration, new values of x and y are found. These inner iterations continue until the differences $x^{(t+1)} - x^{(t)}$ and $y^{(t+1)} - y^{(t)}$ are less than 10^{-6} . From converged x and y values, radii R_1 and R_2 are found. New B_2 value is estimated using R_1 and R_2 , since it is inversely rated with R_2 . Outer iteration continues until the difference between R_1 and R_2 is less than 10^{-7} . One outer iteration step contains two

inner iteration steps for thermal and fast group equations. Table 3.8 shows the first two, 10th and the last two outer iteration steps

Table 3.8 Iteration Steps in Two-Group Problem

Step	B1	B2	R1	R2	R1-R2
1	0.0538777	0.06	42.0489334	39.3658509	2.6830825
2	0.0543778	0.05	41.6380127	47.3828900	5.7448773
10	0.0540664	0.05644	41.8930428	41.8942962	0.0012534
17	0.0540663	0.05644157	41.8931097	41.8931066	3.12286x 10 ⁻⁶
18	0.0540663	0.05644157	41.8931096	41.8931096	6.8311x10 ⁻⁸

Critical radius is found as R=41.8931096cm. Inserting B₂ =0.05644157cm⁻¹ into the (3.65), then gives thermal to fast flux ratio S=0.116309825.

Average fluxes can be calculated from (3.13)

$$\bar{\phi}_1 = \frac{2}{R^2} \int_0^R C_1 J_0(B_1 r) r dr = 0.4820488124 C_1 \quad (3.68)$$

$$\bar{\phi}_2 = \frac{2}{R^2} \int_0^R C_2 J_0(B_2 r) r dr = 0.4462414984 C_2 \quad (3.69)$$

Assume that average thermal to fast flux ratio is equal to thermal to fast flux ratio:

$$C_2 \cong 0.125642148 C_1 \quad (3.70)$$

C₁ and C₂ can be written as

$$C_1 = \frac{P_1}{w_f \Sigma_{f1} \pi R^2 0.4820488124} = 3.3591393 \times 10^9 P_1 \quad (3.71)$$

$$C_2 = \frac{P_2}{w_f \Sigma_{f2} \pi R^2 0.446241498} = 1.6633048 \times 10^8 P_2 \quad (3.72)$$

Thermal and fast power constitute the total reactor power

$$P_1 + P_2 = 2000 \text{W/cm} \quad (3.73)$$

There are four equations with four unknowns. Solutions are P₁=565.3845886W/cm, P₂=1434.615411W/cm, C₁=18.992055x10¹¹, C₂=2.3862027x10¹¹. Fast and thermal fluxes are found from (3.59) and (3.60) approximately.

$$\phi_1 = 18.992055 \times 10^{11} J_0(B_1 r) \quad \text{and} \quad \phi_2 = 2.3862027 \times 10^{11} J_0(B_2 r) \quad (3.74)$$

3.3.2 CNEMR and QFEMR Results

The effective neutron multiplication factors determined by NEM and FEM are given in Table 3.9. Results of this section are quite interesting, for Cubic NEM characteristics change totally.

Table 3.9 Results of QFEMR and CNEMR Programs for Two-Group Reactor

Method	Number of Elements(FEM) or Nodes(NEM)	k_{eff}	Error (%)
Linear FEM	7	1.028537586	2.853759
	10	1.013512079	1.351208
	20	1.003065418	0.306542
	30	1.001166149	0.116615
Quadratic FEM	5	0.999908366	0.009163
	10	0.999663253	0.033675
	15	0.999655302	0.034470
	50	0.999654311	0.034569
Quadratic NEM	2	0.990966845	0.903315
	11	0.999426275	0.057372
	21	0.999611910	0.038809
	31	0.999648762	0.035124
Cubic NEM	6	1.006172820	0.61728
	11	1.001437628	0.14376
	21	1.000150288	0.015028
	31	0.999899120	0.010089

First of all, error percentage values show that Cubic NEM is very impractical for initial nodes because its results are worse than Quadratic FEM and NEM. Traditionally, Linear FEM continues to be the worst and this hasn't changed since the beginning. Secondly, Quadratic FEM shows an unexpected performance when number of elements is 5. Quadratic FEM generally behaves as a fine mesh method; however, the best error percentage value obtained from all trials is the result of Quadratic FEM at 5 elements. Moreover, this is a kind of oscillation because the errors begin to increase, and Cubic NEM becomes the best surprisingly after 14 nodes. By the way, the response of Cubic NEM toward refinement is positive.

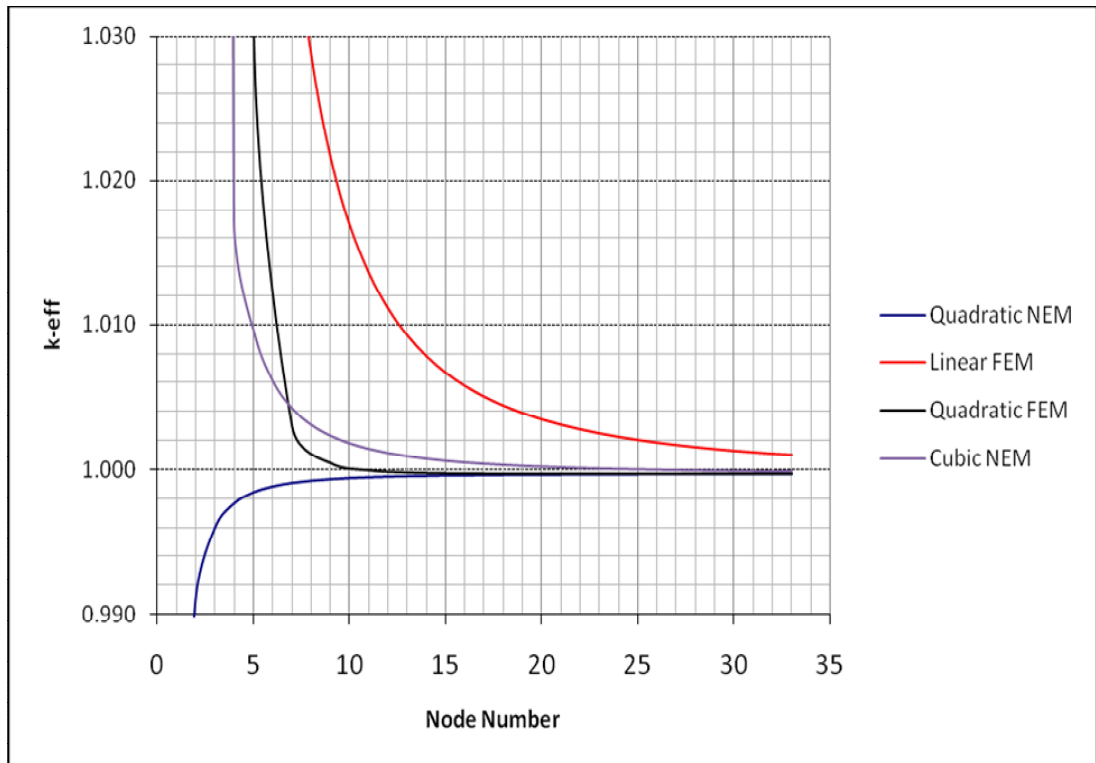


Figure 3.9 k_{eff} Results of FEM and NEM

Another important difference from previous examples occurs in the variation of k_{eff} of Cubic NEM. When the figure 3.9 is examined, again, Quadratic NEM is converging from the values lower than analytical solution, and FEM starts to converge from the values higher than analytical solution. Also, Quadratic NEM is the fastest method, and Linear NEM is the slowest one. In contrast, Cubic NEM shows the similar characteristic with FEM; it is converging from the higher values. Specifically, k_{eff} variation of Cubic NEM seems to Linear FEM for initial nodes, but of course Cubic NEM is faster and more correct.

The error comparison of Quadratic and Cubic NEM is illustrated in figure 3.10. The point that should be emphasized is the slow convergence of Cubic NEM up to 14 nodes. Cubic NEM needs more condensed mesh for this problem in order to be accurate. The increase in the node number affects positively, and Cubic NEM surpasses all other methods in error variation. The change in the characteristic begins exactly after 14 nodes. The rate of change in the error values of Quadratic NEM is small, and it becomes approximately stable after 14 nodes.

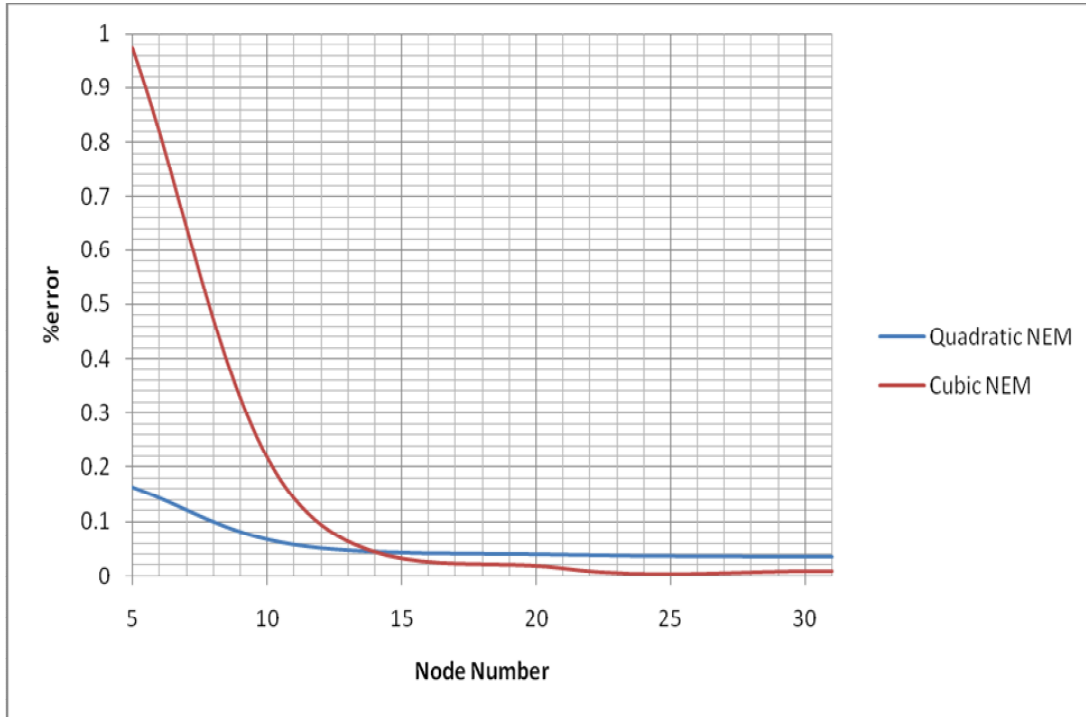


Figure 3.10 k_{eff} %error Variation

Radial Flux variation and comparisons of methods are shown in the figure 3.11 using 31 nodes. Small deviations from analytical solutions exist in the values of both expansions.

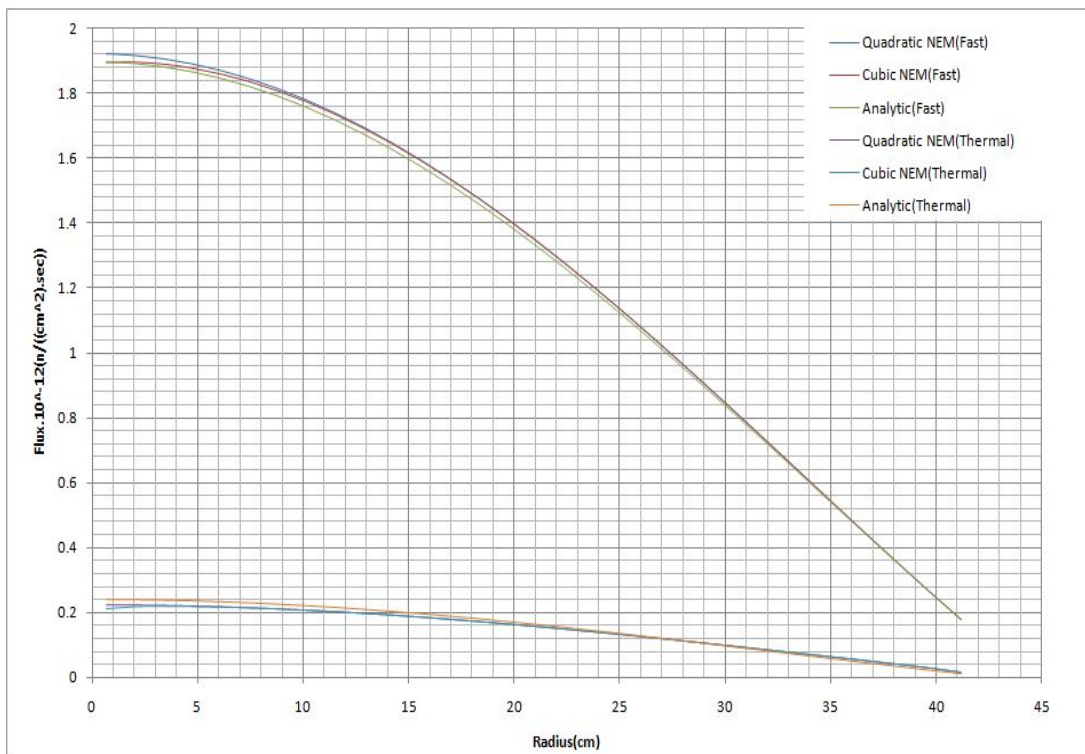


Figure 3.11 Fast and Thermal Flux Distributions

3.4 TRIGA MARK II Reactor

Diffusion theory has been traditionally used for TRIGA whole-core calculations. In this study, one dimensional cylindrical geometry model of TRIGA core is chosen.

Reactor core may be divided into 7 annular regions. Ring A contains only the central thimble. Ring B has 6 fuel elements. Ring C contains 11 fuel elements and one water gap, while ring D has 17 fuel elements and one water gap. Ring E consists of 23 fuel elements and one water gap. Ring F contains 12 fuel elements, 2 water gaps and 16 graphite elements. The core is surrounded by a graphite reflector.

The outer radii of A, B, C, D, E and F rings are 2.1371, 5.9709, 9.8979, 13.8629, 17.7329 and 21.8049 cm's respectively. The graphite reflector outside the F-ring extends to an outer radius of 51.64cm.

The core configuration of the ITU TRIGA MARK II Reactor is given in figure 3.11 [16].

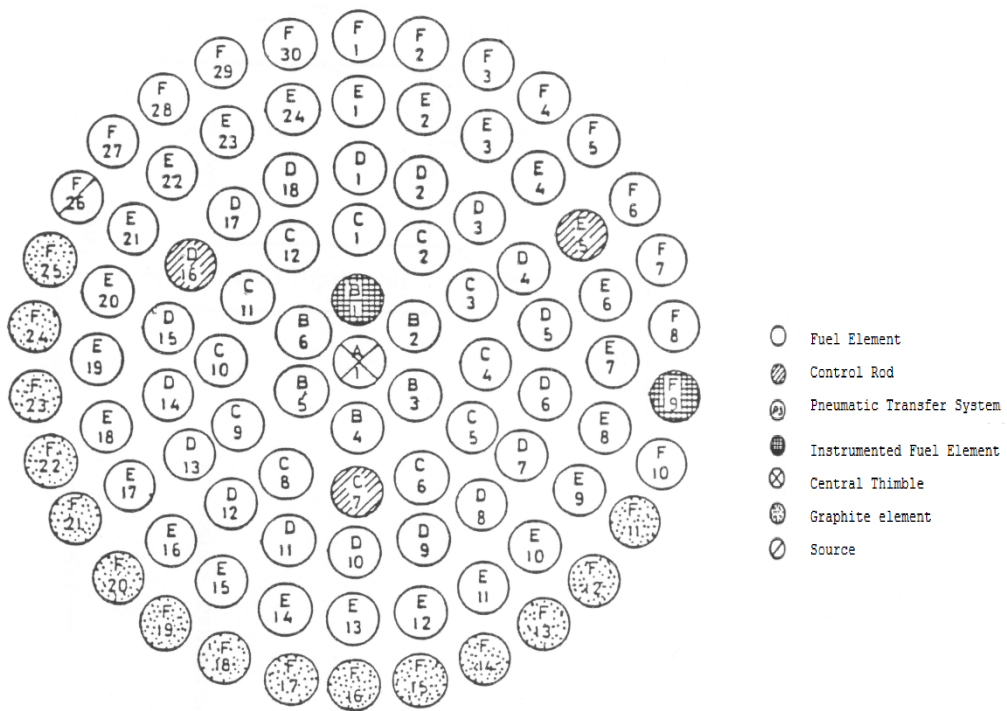


Figure 3.11 ITU TRIGA MARK II Reactor Core Diagram

The homogenized two-group cross-sections for the fuel elements, central thimble, water gap, graphite elements and the graphite reflector has been evaluated using WIMS-D/4 code in a previous study [17]. These cross-sections are subjected to volume averaged homogenization with:

$$\Sigma_{\text{ring}} = \frac{1}{N_{\text{ring}}} \sum_{i=1}^{N_{\text{ring}}} N_i \Sigma_i \quad (3.75)$$

where N_{ring} represented the total number of cells in a ring; N_i , the number of cells type i in the ring. For the diffusion constant, the volume-averaging is done by:

$$D_{\text{ring}} = \frac{N_{\text{ring}}}{\sum_{i=1}^{N_{\text{ring}}} \frac{N_i}{D_i}} \quad (3.76)$$

After the ring homogenizations are done with (3.75) and (3.76), the following cross-section data are obtained. Table 3.10 and 3.11 shows the homogenized fast and thermal cross-sections respectively.

Table 3.10 Homogenized Fast Group Cross-Sections for TRIGA Reactor

Ring	$D_1(\text{cm})$	$\Sigma_{r1}(\text{cm}^{-1})$	$\Sigma_{s1 \rightarrow 2}(\text{cm}^{-1})$	$\nu_1 \Sigma_{f1}(\text{cm}^{-1})$
A	1.21848	0.054012	0.053725	0
B	1.01686	0.048046	0.04267	0.00319902
C	1.02952949	0.04861092	0.04365908	0.00293244
D	1.02527139	0.04842261	0.04332939	0.00302130
E	1.02315553	0.04832846	0.04316454	0.00306573
F	1.19993689	0.03345527	0.03123407	0.00127961
Reflector	1.30156	0.002848	0.002845	0

Table 3.11 Homogenized Thermal Group Cross-Sections for TRIGA Reactor

Ring	$D_2(\text{cm})$	$\Sigma_{a2}(\text{cm}^{-1})$	$\nu_2 \Sigma_{f2}(\text{cm}^{-1})$
A	0.246318	0.01588	0
B	0.244494	0.07921	0.119481
C	0.23985532	0.07394167	0.10952425
D	0.24138186	0.07569778	0.11284317
E	0.24215245	0.07657583	0.11450262
F	0.35853809	0.03561933	0.0477924
Reflector	0.886434	0.000194	0

This data is supplemented with $\nu_1=2.55$, $\nu_2=2.44$, $\chi_1=1$ and $\chi_2=0$. All of them are intended for input to the programs CNEMR and QFEMR.

Then, the node number is chosen as 20 nodes at the beginning. In this basic mesh, there are 1, 2, 3, 3, 3, 2 and 6 nodes in A, B, C, D, E, F rings and the graphite reflector respectively. This mesh strategy seems to be convenient only for Quadratic NEM; however, it doesn't show the same performance for Cubic NEM. For that

reason, 2 different basic meshes are applied for the expansions of different degrees. The basic mesh of Cubic NEM contains 1, 3, 4, 4, 4, 3, 6 nodes respectively in 7 regions. By multiplying the number of annular regions in the basic mesh by an integer (degree of refinement), finer meshes may be produced. In QFEMR finest mesh consists of 641 nodes which correspond to 640 linear elements and 320 quadratic elements. QFEMR with 320 quadratic elements or 16 degree of refinement gives $k_{\text{eff}}=1.21051196$. Quadratic FEM gives more exact results as shown in the previous problems when the number of elements is increased. Considering the finest Quadratic FEM data as reference value, Table 3.12 shows the effective neutron multiplication factors with their errors.

Using 20 nodes (1, 2, 3, 3, 3, 2, 6), Quadratic NEM finds the effective multiplication factor as $k_{\text{eff}}=1.21054283$. The k_{eff} calculated by Cubic NEM is 1.21021145. Linear QFEMR and quadratic QFEMR find $k_{\text{eff}}=1.21279558$ and $k_{\text{eff}}=1.21052344$ with 20 elements respectively. The error percentage of Quadratic NEM is approximately 10 times better than Cubic NEM value.

Using 25 nodes (1, 3, 4, 4, 4, 3, 6), Quadratic NEM error percentage is higher than its value with 20 nodes although the node number is increased. Cubic NEM result is 40 times better than Quadratic NEM value. The cause of this effect is that both methods behave exactly like a fine mesh method. Not only the node number, but also mesh strategy is very important for multigroup problems. Especially, when FDM is applied, if the mesh doesn't fit on geometry, one can observe incoherent results.

Cubic NEM performs to have %0.0001008 at 50 nodes, and this validates that CNEMR can calculate effective multiplication factors of the TRIGA-like two-group, multiregional systems with a small error.

Table 3.12 CNEMR k_{eff} Results for Different Meshes in TRIGA Reactor

Nodes		Quadratic NEM		Cubic NEM	
Mesh	Total Nodes	k_{eff}	Error(%)	k_{eff}	Error(%)
1x2x3x3x3x2x6	20	1.21054283	0.00255016	1.21021145	0.0248249
1x3x4x4x4x3x6	25	1.21072643	0.01771730	1.21046235	0.0040983
2x4x6x6x6x4x12	40	1.21052886	0.00139610	1.21045264	0.0049004
2x6x8x8x8x6x12	50	1.21057897	0.00553567	1.21051074	0.0001008

Figure 3.12 shows the fast and thermal flux distributions from CNEMR. Reactor thermal power is taken to be 1000W/cm. These flux profiles are very similar to the results of previous studies [13]. A straight line shows the boundary between the fuel region and the reflector at 21.8 cm.

Figure 3.13 shows linear QFEMR results with 640 elements. CNEMR and linear QFEMR flux profiles are very close to each other.

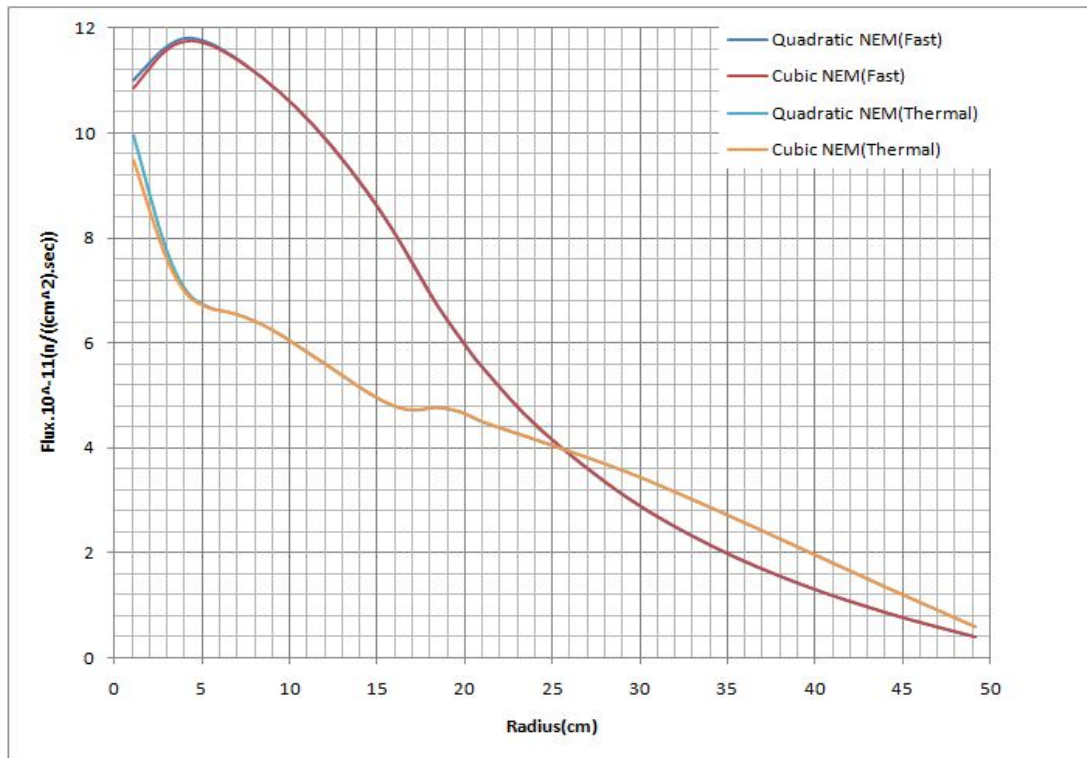


Figure 3.12 TRIGA Reactor Flux Distribution (CNEMR)

Fast and thermal group average fluxes are calculated by CNEMR with 50 nodes as

$$\bar{\phi}_F = 0.5115984987 \times 10^{12} \text{ neutrons/cm}^2 \text{ sec.}$$

$$\bar{\phi}_T = 0.3703848362 \times 10^{12} \text{ neutrons/cm}^2 \text{ sec.}$$

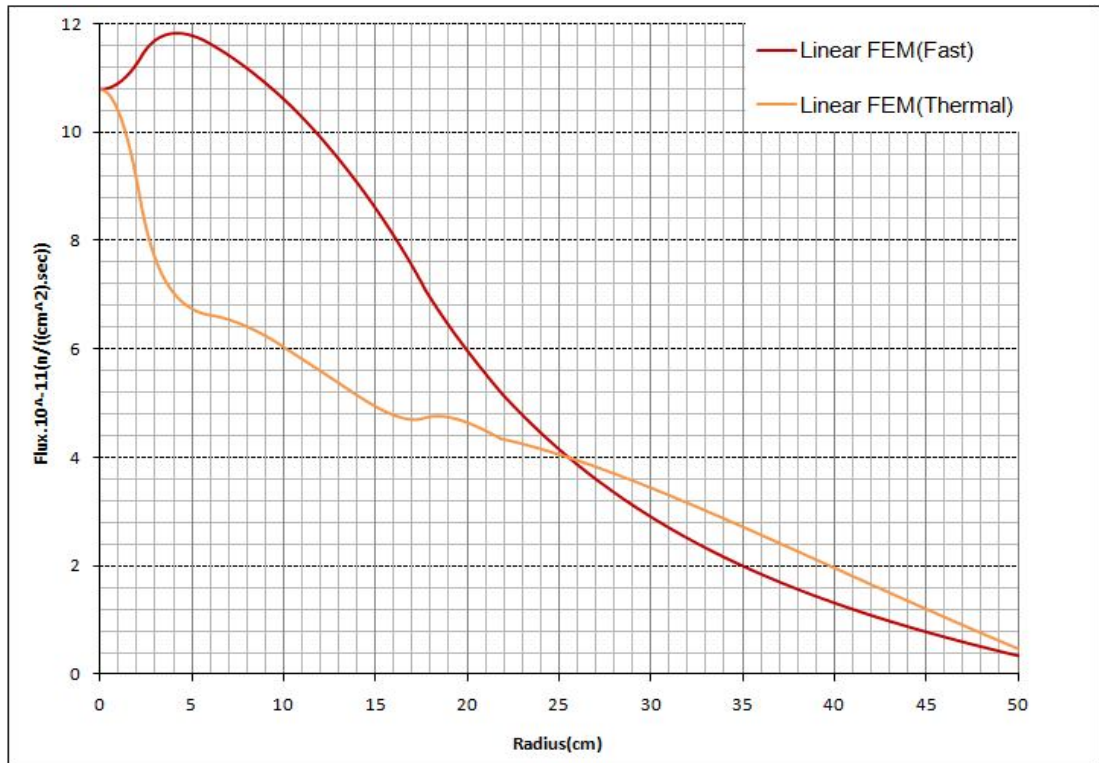


Figure 3.13 TRIGA Reactor Flux Distribution (Linear QFEMR)

Finally, ring averaged fluxes are given in table 3.13. Similar results are obtained with the finest mesh linear QFEMR.

Table 3.13 Ring Averaged Fluxes of TRIGA Reactor

Average Fluxes	Quadratic NEM (2x6x8x8x8x6x12)		Cubic NEM (2x6x8x8x8x6x12)		Linear FEM (finest, 640 elements)	
	Fast Flux $\bar{\phi}_F \times 10^{-11}$	Thermal Flux $\bar{\phi}_T \times 10^{-11}$	Fast Flux $\bar{\phi}_F \times 10^{-11}$	Thermal Flux $\bar{\phi}_T \times 10^{-11}$	Fast Flux $\bar{\phi}_F \times 10^{-11}$	Thermal Flux $\bar{\phi}_T \times 10^{-11}$
A	11.06090	9.85227	11.02715	9.74307	11.07604	9.8165
B	11.74338	7.07840	11.72994	7.06320	11.74535	7.0797
C	11.14001	6.37665	11.13714	6.37682	11.14006	6.3775
D	9.88907	5.59886	9.88998	5.60023	9.88817	5.5988
E	8.12078	4.84942	8.12201	4.85135	8.11869	4.8495
F	6.06031	4.62868	6.06090	4.63061	6.05777	4.6272
Reflector	1.72135	2.13119	1.72296	2.13150	1.72210	2.1299

4 CONCLUSION

Present study is the application of a high order Nodal Expansion, Cubic NEM, to the neutron diffusion equation in cylindrical geometry. NEM provides the opportunity of precision selection, which is defined by the degree of the basis polynomials. The same advantage exists in Finite Element Method with the decision on the degree of Elements. On the other hand, Finite Difference Method is just categorized as forward, backward, and mesh centered difference.

High order and low order Nodal expansions have common and different points during the derivation of the iterative system. First of all, the common steps are Nodal Balance Equation and usage of Fick's law with partial neutron currents. Both expansions require these two steps in order to find the necessary unknowns. However, the differences outweigh the similarities. The first difference is that Fick's Law and Nodal Balance equation are sufficient to derive the system of low order expansion; in contrast, Cubic Expansion needs a supplementary expression in order to find expansion coefficient because n^{th} order expansion needs to have $n+1$ basis polynomials and expansion coefficients. Hence, first moment of neutron flux should be determined in order to calculate the expansion coefficients. The second difference is the recalculation of the expansion coefficients. Each order of expansion causes changes in the coefficient terms, and the coefficients are getting more complicated as the degree of expansion is increasing. Another important difference is the requirement of weighted residual technique. The unknowns of Quadratic NEM are the outgoing partial currents ($J_{i+1/2}^+, J_{i-1/2}^-$), the node flux ϕ_i for each node, so Quadratic NEM has $3N \times 3N$ matrix system due to its 3 unknowns per node. However, the first moment of neutron flux is added in Cubic NEM. This means that the number of the unknowns becomes 4 per node, and the dimension of the response matrix will be $4N \times 4N$. At this point, the remaining equation is obtained by the first moment of neutron diffusion equation.

After the derivation of the response matrix and the matrix system is implemented to the CNEMR code, which is able to realize Quadratic and Cubic NEM in FORTRAN. A finite element method program, namely QFEMR was used in order to compare Nodal Expansion Method with Linear and Quadratic Finite Element methods. CNEMR was tested by running four benchmarking problems and making comparisons with analytical solutions. In order to find solutions, other numerical methods are also used: Newton Method for transcendental relations in analytical solutions, Fission Source Power Iteration for the eigenvalue of the system, and linear solvers.

The comparisons are based on the calculation of effective neutron multiplication factors, average fluxes for each group and the material with their errors. Moreover, flux distributions are illustrated and compared with Quadratic NEM.

The comparisons reveal that convergence of Cubic NEM to acceptable values is faster than the compared methods in one-group problems, and the augmentation of node number results in the decrement of error. However, Cubic NEM behaves like a fine mesh method in 2-group examples. Besides slow convergence, error is decreasing sharply with respect to the increment of the node number, and it gets best results in terms of error versus its rivals after the node number reaches the saturation level.

One can consider Cubic NEM as an intermediate method between Quadratic NEM and Quadratic FEM for two reasons, and actually it contains the advantages of both these methods. The first reason is that Cubic NEM may be considered slower with respect to Quadratic NEM, but it is faster than Quadratic FEM. The other reason is that the response of Quadratic NEM is not positive for refinement because the error variation is so slow. However, Cubic NEM always shows nice results when the refinement occurs.

All in all, Cubic NEM can be preferred instead of FEM in order to get fast “acceptable” results, and it is more attractive than Quadratic NEM with the freedom in error precision. It shouldn’t be forgotten that this decision depends on your computer configuration, your time, and your tolerance for error.

REFERENCES

- [1] **Huang, K.**, 1987. Statistical Mechanics, Wiley.
- [2] **Lamarsh, J. R.**, 1983. Introduction to Nuclear Engineering, Addison-Wesley, Reading, Massachusetts.
- [3] **Zienkiewicz, O. C., Taylor, R. L., Zhu, J. Z.**, 2005. The Finite Element Method: Its Basis and Fundamentals, Sixth Edition, Elsevier.
- [4] **Kang, C. M., Hansen, K. F.**, 1973. Finite Element Methods for Reactor Analysis, Nucl. Sci. Eng. 51 (456).
- [5] **Bennewitz, F., Finnemann, H., and Moldschl, H.**, 1975. Solution of the Multidimensional Neutron Diffusion Equation by Nodal Expansion, Proc. Conf. Computational Methods in Nuclear Engineering, 1-99 CONF-750413 ANS, Charleston, S.C.
- [6] **Gamino, R. G.**, 1986. "The Development and Application of Supernodal Methods to PWR Analysis," Thesis, Dept. of Nucl. Eng. MIT.
- [7] **Henry, A. F.**, 1972. Refinements in Accuracy of Coarse Mesh Finite-Difference Solution of Group-Diffusion Equations," Proc. Seminar on Numerical Reactor Calculations, 447 IAEA.
- [8] **Bennewitz, F., Finnemann, H., and Wagner, M.**, 1975. High Order Corrections in Nodal Reactor Calculations. Trans. Am. Nucl. 22 250.
- [9] **Stacey, W. M.**, 2001. Nuclear Reactor Physics, John Wiley and Sons INC., New York.
- [10] **Finnemann, H., Bennewitz, F., and Wagner, M. R.**, 1977. Interface Currents Techniques for Multidimensional Reactor Calculations, Atomkernenergie, 30, 123.
- [11] **Finlayson, B. A., and Soriven, L. E.**, 1966. The Method of Weighted Residuals—A Review. Applied Mechanics Reviews, Vol. 19, No 9.
- [12] **Duderstadt, J. J., and Martin, W. R.**, 1979. Transport Theory. Wiley
- [13] **Mercimek, M., and Özgener, H. A.**, 2008. Development of a nodal method for the solution of the neutron diffusion equation in cylindrical geometry, The Fifth Eurasian Conference on Nuclear Science and Its Applications.
- [14] <http://www.netlib.org/linpack/dgbsl.f>, <http://www.netlib.org/linpack/dgbfa.f>
- [15] **Hoffman, J. D.**, 2001. Numerical Methods for Engineers and Scientists. Marcel Dekker, Inc., New York-Basel.
- [16] **Safety Analysis Report for the ITU TRIGA MARK II Reactor.** 1978.
- [17] **Ozgener, H. A., Ozgener, B., and Buke T.**, 1999. A comparison of integral transport and diffusion theory methods in whole core TRIGA calculations, VTT Symposium, 197, 27-38.

APPENDIX A A MANUAL FOR CNEMR

A.1 INPUT LIST

CARD 1

- NGT** : Number of energy groups.
- MAT** : Number of materials.
- NETSOR** : Free neutron source. It is 1, if the free neutron source exists in the system. It is 0 otherwise.
- NRBCT** : Boundary condition. It is 1, if the boundary condition is zero incoming current at the boundary.
- Ord** : Order of Nodal Expansion. It is 2 for Quadratic Expansion, 3 for Cubic Expansion.

CARD 2

- ITMAX** : Maximum number of iterations.
- EPS** : Convergence parameter.
- ENGEN1** : Initial estimate of effective multiplication factor.

CARD 3

- SKAY(I, J)** : Free neutron source of I^{th} group and J^{th} material. Every line indicates the material number and every given number in a line is for the energy group of that material. CNEMR skips this card if NETSOR is given zero.

CARD 4

- D(I,J)** : Diffusion coefficients for I^{th} group and J^{th} material.

CARD 5

- CEKES(I,J)** : Removal cross-sections for I^{th} group and J^{th} material.

CARD 6

- SEKES(I,K,J)** : Scattering cross-sections from group K to the group I for J^{th} material.

CARD 7

- FEKES(I,J)** : Fission reaction cross-section. $\nu\Sigma_f$ for I^{th} group and J^{th} material.

CARD 8

- FEKES1(I,J)** : Fission cross-section, Σ_f for I^{th} group and J^{th} material.

Card 4,5,6,7 and 8 are repeated for each material.

CARD 9

SFIS(I) : Fission spectrum, χ for I^{th} group.

CARD 10

NOD (I) : Number of nodes in I^{th} material.

CARD 11

RDIS(I) : Outer radius of I^{th} material.

CARD 12

P : Reactor thermal power in Watts/cm.

A.2 DESCRIPTION OF CNEMR SUBROUTINES

SKINP : Reads the free source values for each group and the material from the input file.

INPUT : Reads the cross-sections, fission spectrums, number of nodes for each material and the material outer radii from the input file and writes to the output file.

FISSOR : Makes the fission source iteration.

MATRIS : Calculates the elements of matrix A described in the equation (2.114) for the zero incoming current for all expansions and reflective boundary conditions for Quadratic Expansion. All elements of the matrix A were described in section (2.5).

SCASOR : Free source and scattering terms of the nodal balance equation are calculated with this routine. B1 contains these terms. Adding B1 from this routine and B2 from FISSOR constitutes new B2 which is the RHS of matrix equation.

DGBF : Factors a double precision band matrix by elimination. ABD contains the matrix in band storage

On return, ABD is an upper triangular matrix in band storage and the multipliers which were used to obtain it. The factorization can be written $A = L*U$ where L is a product of permutation and unit lower triangular matrices and U is upper triangular. IPVT contains the pivot indices.

If info returns info=0, this is the normal value. It equals to k if U(k, k) equals to 0.0. This is not an error condition for this subroutine, but indicates that DGBSL will divide by zero if called.

DGBF calls the subroutines DAXPY and DSCAL and the integer function IDAMAX.

DAXPY : It returns constant times a vector plus a vector. It uses unrolled loops for increments equal to one.

IDAMAX : Finds the smallest index of that component of a vector having the maximum magnitude.

- DSCAL** : Scales a vector by a constant. It uses unrolled loops for increment equals to one.
- DGBSL** : Solves the double precision band system $Ax=B$ using the factors computed by DGBFA. B is the RHS vector. On return, it gives the solution vector B. It calls subroutine DAXPY.
- AVG** : Calculates the average fluxes for each material and group. AFLUX is the group averaged flux and AF is material averaged flux.
- OUTPUT** : First calculates, the constant A described (3.16) for the problem 1. Then, flux distribution with respect to the radius is found. Last, averaged fluxes are written into the output file.

Important Note:

The maximum node number that can be used for runs is 50 for Cubic Expansion, and 66 for Quadratic Expansion. Also, the group number can be increased up to 10, and the diversity of the materials can be divided into 10 regions. Additionally, Cubic expansion requires a supplementary array for Neutron Flux Moments, and it is selected as MOM (I, J).

APPENDIX B COMPUTER PROGRAMS

CNEMR and QFEMR programs with input files for the problems considered in this study are given in an enclosed CD.

RESUME



He was born in Istanbul at 1982. He was graduated from Saint-Benoit French School in 2001. He got his B.S in Physics from Işık University in 2006.

Permanent Address: Dikilitaş, Gelincik Sokak, Başak apartmanı, no:2 daire:2

Beşiktaş\İstanbul